Manuscript (2002), **met.no 01/03**, pp. 1–46

Downscaling analysis for daily and monthly values using *clim.pact-V.0.9*.

By Rasmus E. Benestad

The Norwegian Meteorological Institute, PO Box 43, 0313, Oslo, Norway *

January 7, 2003

ABSTRACT

An analysis tool, `clim.pact`*, has been developed for empirical downscaling and analysis of local and regional climate on both a daily and a monthly basis. This tool is tested with both monthly and daily data and a number of different scenarios are compared.*

Empirical downscaling is carried out with `clim.pact` *on January mean temperature in Bergen, Copenhagen, Helsinki, Oslo, Stockholm, and Tromsø, using single field as well as mixed-field predictors and with predictors that cover different regions. A comparison is made between the various results in order to study the robustness of the method. Furthermore, the residuals from the model calibration are examined for remaining trends or biases.*

The `clim.pact` *package is used for downscaling of daily winter mean temperature and precipitation in Bergen and Oslo. The statistical relationship between the regional climate and local variability is examined and future shifts in mean and extreme values, suggested by the scenarios, are presented.*

KEY WORDS: Downscaling analysis Daily values Monthly values common EOFs.

* *Corresponding author: R.E. Benestad, rasmus.benestad@met.no, The Norwegian Meteorological Institute, PO Box 43, 0313 Oslo, Norway, phone +47-22 96 31 70, fax +47-22 96 30 50*

Contents

1 Introduction

In 1896, Svante A. Arrhenius (*Arrhenius*, 1896) proposed that atmospheric CO_2 may have a warming effect on Earth's surface. There has been a gradual accumulation of the carbon dioxide concentrations in the atmosphere (*IPCC*, 2001) as well as other so-called "greenhouse gases" since the industrial revolution. This build-up leads to a perturbation in the energy balance between the incoming solar radiation and the infrared radiation emitted from Earth's surface, and there are concerns about the effects of such an energy imbalance on our climate. A climate change has potentially severe consequences for the society, and it is therefore important to be able to forecast future climatic trends. Although the nature of the climate system is chaotic (*Lorenz*, 1967) and its exact trajectory cannot be deterministically predicted years ahead, it may nevertheless be possible to predict the long-term climatic trends, given a systematic change in the boundary conditions. Such predictions are based on coupled atmosphere-ocean general circulation models (AOGCMs), which describe the large-scale dynamics and thermodynamics of the climate systems. The term "climate scenarios" is used henceforth in order to emphasis the fact that these climate models only can forecast plausible climatic trends and that the internal variations are more arbitrary. Estimations of globally averaged temperature indicate warming over the past century (*IPCC*, 2001). Although the global aspect of a climate change is important for monitoring purposes and the understanding of our climate, it is the local climate shifts that will have direct effects on our future. Therefore, it is important to consider which implications a global warming may have for regional climates.

The most recent global coupled atmosphere-ocean general circulation models (AOGCMs) tend to give a realistic description of the large-scale climatic features, such as the mean circulation patterns (i.e. the Hadley Cell and westerlies in the mid-latitudes), the coupled ocean-atmosphere processes in the tropics associated El Niño Southern Oscillation (ENSO) (*Collins*, 2000), and the shifts in the air masses often referred to as the North Atlantic Oscillation (NAO). But, the model topography has until now been crude, and features such as the Norwegian mountain ranges have not been represented realistically in these models (see Figure 1). It is then no surprise that even the most recent AOGCM cannot give a good detailed description of regional climatic features. Analytical results from *Grotch & MacCracken* (1991) may suggest that the global climate models cannot give a good description of features smaller than sub-continental scales.

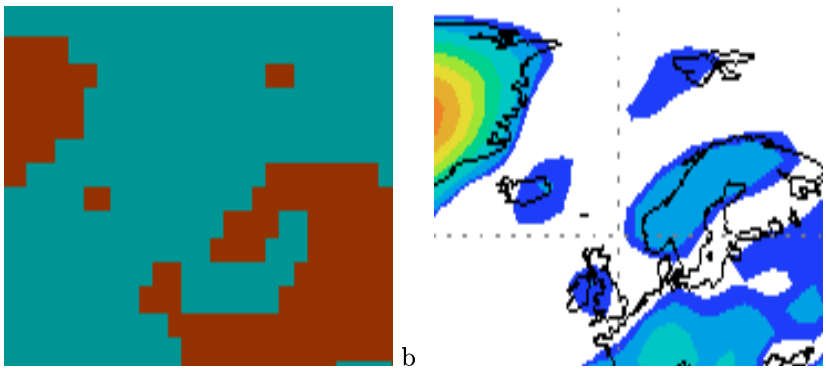

Figure 1. The land-sea mask for the Nordic countries used in the ECHAM4 model (a) and the ECHAM4 model topography (b). [The figures were obtained from the IPCC Web site].

Despite the caveats about the grid-scale representation of climate, it may still be possible to use the AOGCMs to describe local climate characteristics if the local climate is affected by large-scale features. Moreover, there may be information in large-scale climate anomalies that can be used to infer local climate variability. However, this requires extra knowledge about how the large-scale climatic features relate to the local climate variables. So-called downscaling models, based on either physical considerations (nested dynamical models used in dynamical downscaling (*Bjørge* et al., 2000; *Christensen* et al., 1998)) or empirical studies (empirical or statistical downscaling) can be used to relate the large scale climatic patterns to local scales. Here, we will focus on the empirical downscaling approach. Empirical models are based on statistical relationships between the local climate variations and large-scale climate anomalies (*Zorita & von Storch*, 1997; *Kidson & Thompson*, 1998; *Heyen* et al., 1996; *Wilby* et al., 1998; *Crane &*

Hewitson, 1998). Empirical downscaling has often used principal component analysis (PCA) to reduce the degrees of freedom. The PCA products are ideal for regression type analysis because the set of PCA timeseries are mutually orthogonal. It is important to note that the empirical models assume that the historical relations between large-scale and local climate anomalies also will be true for the future. This "assumption of invariability" implies that there is some degree of uncertainty attached to the empirically downscaled scenarios due to the possibility of future changes in the relationship between large and small scales. This assumption can be tested to some degree through a two-step process: *a)* calibrating a downscaling model on a subsection of the observations and using the remaining part of the record for validation, and *b)* training the downscaling model on a subsection ("1860-1991") of the AOGCM results and a corresponding grid point value, then using the "1990-2049" for validation. Evaluations carried out on the ECHAM4-GSDIO scenario by *Benestad* (2001b) suggests that the relationship between the large-scale anomalies and local climate variations is only slightly non-stationary, and that empirical downscaling will give realistic results.

Downscaling analysis can provide more than just the local scenarios. Depending on the downscaling strategy, it is possible to incorporate a type of quality control by searching for the same spatial structures in the model simulations as those identified in the actual climate to have an association with local climate anomalies. Thus, by comparing the similarities of the spatial patterns, their spectral properties, and the variance accounted by these, it is possible to make some assessment of the quality of the model results. Downscaling based on common EOFs provides a measure for how realistically the climate model describes the geographical distribution of the climate variables.

There are error sources other than the invariability assumption which increase the uncertainty associated with the prediction of future climates. The sources of uncertainties may be classified as *i)* uncertainties about future emission scenarios, *ii)* climate model shortcomings, *iii)* internal variability, and *iv)* additional errors introduced by the downscaling analysis.

The category "greenhouse gas emission" *(i)* is based on economics considerations and scenarios, which are outside the scope of this study. Climate model shortcomings *(ii)* may imply systematic biases, for instance due to crude description of unresolved processes using statistical parameterisation schemes (also commonly referred to as "model physics"). The imperfect description of clouds in the climate models is one of the most important sources of uncertainties (*IPCC*, 2001). Another example of such model shortcomings is the artificial climate drift, which is a mismatch in the fluxes between the atmosphere and oceans described by the atmospheric and oceanic models. Yet another example of possible climate model shortcomings may involve the description of sea-ice (*Meehl* et al., 2000; *Benestad* et al., 2002). *Parkinson* et al. (2001) conducted a series of experiments with a climate model and reported high sensitivity to variations in the sea-ice concentrations in the Arctic, and even errors in the satellite-derived sea-ice products can lead to significant differences in model climates. A 66% reduction in the sea-ice concentration was reported to give as much as 30°C increase in polar regions. Thus, different sea-ice conditions associated with the different model climates may be one important source of uncertainty. *Shindell* et al. (2001) found important differences between climate models which include and exclude a detailed description of the stratosphere. Hence, the omission of stratospheric processes common among many climate models, used for enhanced greenhouse gas studies, may increase the uncertainties associated with climate model shortcomings. Finally, the invariability assumption also applies to all parameterisation schemes relying on a statistical description of sub-grid point scales, and non-stationarity in the relationships described by such schemes may in fact be a greater problem than for the empirical downscaling schemes. Furthermore, any such non-stationarity may vary with the spatial resolution

Although empirical downscaling cannot address uncertainties stemming from possible errors in emission scenarios and climate model shortcomings *(i–ii)*, uncertainties associated with internal variations *(iii)*, or natural fluctuations, can be estimated from the standard error in slope estimate (*Press* et al., 1989, eg. 14.2.9) which is usually available from standard data analysis tools. Furthermore, trend analysis may involve polynomial expressions (*Benestad*, 2002b) in order to describe slow variations in the record, such as the rapid warming in northern Scandinavia during 1900–1930 and the slight cooling during 1940–1960.

Although, the climate simulations bear a time stamp in form of the forcing record, the translation between model dates and actual dates is not well defined due to poorly known climatic state in 1860 and arbitrary spin-up processes. This matter is partly related to the strong natural variability on decadal time scales in the high latitudes which affect the trend analysis. A distinction will therefore be made in

this paper between the actual time and the model date by expressing the model dates in apostrophes. Thus, the year 1960 means the real date with which historical observations may be associated, whereas the model year "1960" denotes a year in the model simulations which is meant to describe a model climate analogous to the actual 1960 climate.

This report evaluates and documents `clim.pact`, an analytical tool for empirical downscaling. This tool has been developed in a data-processing language `R`* (a GNU product that is similar to S-plus). The details of the empirical downscaling are given section (2) and the evaluation of this tool are presented in section (3). The `clim.pact` is currently being evaluated in downscaling studies under the Arctic Climate Impact Assessment (ACIA) project†, and is still under development. Version 0.9 of `clim.pact` contains linear models for downscaling, but there are plans to incorporate additional functions, including neural nets and possible analogue methods before version 1.0 is ready. It is also important to have `clim.pact` thoroughly tested before version 1.0 is released.

2 Methods & Data

2.1 Methods

The `clim.pact` package contains a number of different functions and data sets. The downscaling is carried out in two steps: (i) carry out a PCA; (ii) use the PCA products as predictors for the downscaling. There are four different functions in `clim.pact` that carry out different varieties of PCA: (i) `eof.c()`, (ii) `eof.mc()`, (iii) `eof.dc()`, and (iv) `eof.dmc()`. The two former are applied to monthly mean values whereas the two latter are used for daily values (suffix starting with "d" denotes daily values). The `eof.c()` and `eof.dc()` functions produce common EOFs (*Flury*, 1988; *Sengupta & Boyle*, 1993, 1998; *Barnett*, 1999; *Benestad*, 2001b,c, 2002a) whereas `eof.mc()` and `eof.dmc()` produce mixed-field common EOFs (*Benestad* et al., 2002). In the latter type, two fields, such as surface air temperature and sea level pressure, are standardised (by the a common mean and standard deviation estimated from all the grid-box values of the observations) and then combined at each time of observation to form a vector with a length equal to the sum of the lengths of the individual grids. A geographical weighting function is applied to ensure that the contribution of grid grid-box is proportional to its surface area. The data has not been sub-sampled in time, as recommended by *North* et al. (1982). In the case of monthly mean values, the PCA is applied to one month a year (e.g. January mean values), and there is little year-to-year correlation. The daily values may have significant auto-correlation, but since the PCA is not intended as the final product in a statistical analysis, but rather as a preliminary product used as input for the downscaling, it is not important that each observation in time should be independent. PCA here is merely used for the compression of information and to ensure that the downscaling is based on the same spatial patterns in both the real world and the model simulations.

There are two main functions `ds()` and `ds.dm()` which carry out actual the downscaling ("ds" is an abbreviation for downscaling, and the suffix "dm" refers to daily mean). The downscaling can be done for temperature, rainfall, or any other variable or index that exhibit a real and significant statistical relationship with the predictor. It is important that the presentation of the downscaling results are accompanied by a discussion on plausible physical explanations for a relationship between the predictors and the predictand.

The `clim.pact` also contains functions for plotting climate station data (`plot.nordklim()` which is now more general than just plotting data from the Nordklim data set: time series and histogram/p.d.f.) as well as data retrieval (`getnacd()` and `getnordklim()`). The data-retrieval functions usually assume that the data is residing in a sub-directory (default "data/"). The manual for `clim.pact` is reproduced in the appendix, giving the complete listing of functions and data sets contained in this package.

2.2 Monthly mean values

The monthly downscaling is based on a step-wise (`R` function `step()`) regression and is optimized when the Akaike information criterion (AIC) (*Wilks*, 1995, 300–302) is minimized. The optimisation of the

*URL: http://cran.r-project.org.
†http://www.iarc.uaf.edu/acia.html

model is based on the 8 leading modes and the final selection depends on the combination that yields the lowest AIC. Prior to the regression, the principal components corresponding to the observations and the station record are de-trended (*Benestad*, 1999, 2001a) (the model data is of course not de-trended).

The downscaling on monthly data expresses climatic changes in terms of long-term trends. Both linear and fifth-order polynomial trends are estimated using a regression against time (a time-index is used which is vector that has the same length as the record, but with values between -1 and 1: $t \in [-1, 1]$, (*Benestad*, 2002b)). The analysis also incorporates the residuals from the regression analysis associated with the model calibration. Any "structure" (e.g. bias in distribution, preferred time scales, autocorrelation, or trends) in the residual may indicate that the downscaling model does not give a good representation of the local climate.

2.3 Daily mean values

The downscaling for daily values uses a regression approach similar to the monthly values, but the 20 of the leading modes are used in the step-wise screening. The reason for choosing a higher number of modes for daily downscaling than for monthly downscaling is: (i) that weather systems of smaller spatial scales may have a greater impact on shorter time scales and (ii) the length of the daily record is ~ 4000 observations, whereas corresponding the corresponding length for the monthly values ~ 100. The data are not de-trended prior to the downscaling, but the variations associated with the annual cycle are subtracted. The annual cycle is estimated as the best-fit of a regression of three annual harmonics to the original data:

$$\hat{y}(t) = c_0 + c_1 \cos(\omega t) + c_2 \sin(\omega t) + c_3 \cos(2\omega t) + c_4 \sin(2\omega t) + c_5 \cos(3\omega t) + c_6 \sin(3\omega t), \qquad (1)$$

where $\omega = 2\pi/(365.25\text{days})$ and t is the Julian day. After the annual cycle has been reconstructed and removed from the data (in `eof.dc()`, `eof.dmc()`, and `ds.dm()`), the data of a given season is extracted (e.g. December–January values only) and used as inputs for the downscaling analysis.

The downscaling of daily values does not involve trend analysis because of following reasons: (i) the daily data usually involve much larger data sets than monthly mean values; (ii) the daily records are usually much shorter than the monthly data; and (iii) the daily data often is given in the form of two time-slices representing a control period and the future scenario. The function `ds.dm()` assumes that the daily data contains two time slices, and automatically assigns the data with dates before year 2000 to the control period and the data with the time-stamp greater than year 2000 is assumed to be the scenario.

One limitation of downscaling using linear empirical models is that the downscaled results must have a similar distribution (Gaussian) as the predictors. The daily rainfall is non-Gaussian, but the time series representing the large-scale anomalies tend to be approximately normally distributed. Furthermore, least-squares optimisation algorithms often assume that the data is normally distributed. Thus, the downscaling of daily precipitation is problematic when it is not normally distributed. A transformation is carried out in the attempt to normalize (get a representation that is normally distributed) the data. Here, a simple log-transformation is used, but in principle, and type of transformation can be used. Quantile-quantile plots (qq-plots) are used for assessing how close the data are to being normally distributed.

The relationship between the local variability and the regional-scale climate can be examined through the means of scatter plots showing the actual station record and the predicted values from the model calibration. A good fit (tight clustering about the diagonal, high R^2 value and low p-value) gives confidence in using the model. The residuals from the regression are also plotted in order to examine whether the downscaling models fail to capture significant features.

The downscaling analysis incorporates a comparison between the distributions of control and scenario data and fit Gaussian p.d.f.s to these. The downscaling of the daily values incorporates extreme-value analysis, using the `R`-package `gev` to fit the tails of a general extreme value (GEV) distribution function. An r-largest order statistics method (*Coles*, 1999) has been adopted where the 7 highest numbers are selected per year.

2.4 Data

The predictor data for the monthly values used in these tests are based on the re-analysis from the National Center for Environmental Prediction (NCEP) in USA (*Kalnay* et al., 1996) and model results from the ECHAM4/OPYC3 GSDIO (IS92a greenhouse gases, direct and indirect effects of aerosols (sulfur), and tropospheric ozone) experiment carried out by the Max-Planck Institute for Meteorology (Hamburg, Germany). For daily predictor data, the predictors were derived from the European Centre for Medium-range Weather Forecasts (ECMWF) re-analysis (ERA-15) (*Gibson* et al., 1997) and results from dynamical downscaling of the ECHAM4/OPYC3 GSDIO scenario using the HIRHAM model (*Bjørge* et al., 2000) (carried out at the Norwegian Meteorological institute). The daily ERA-15 were estimated taking the mean of instantaneous values at 00.00 06.00 12.00 18.00 UTC.

The predictand data for the monthly analysis were taken from the Nordklim data set (*Tuomenvirta* et al., 2001) and the Norwegian Meteorological institute climate data base (Cuouddatmohkki) while the daily data were all taken from the Norwegian Meteorological institute climate data base. The Nordklim data are homogeneous and have been subject to thorough quality tests.

The daily station records contain 24-hour averages estimated for the daily intervals 18.00–18.00 UTC (19.00–19.00 local time) for temperature, starting the "previous" day according to the day stamp. The estimate of the mean value was based on 3 observations per day (18.00,06.00,12.00) based on a formula by Køppen: $\overline{T}_{\text{day}} = T_f - k(T_f - T_n)$. The symbol T_f is the mean of the temperature 3 measurements, T_n is the minimum temperature, and k is a function of location, season and observation times (the Køppen parameter). These data are met.no's "official daily mean" values, taken from met.no's climate data archive*. For precipitation, the daily mean value is measured over the 24-hour period 06.00–06.00 UTC (readings made in the morning), starting the same day as indicated by the time stamp.

3 Results

3.1 Monthly mean temperature

3.1.1 Differences caused by different predictor area

Figure 2 shows the results from downscaling at Bergen (a), Copenhagen (b), Helsinki (c), Oslo (d), Stockholm (e) and Tromsø based on surface air temperatures over most of the North Atlantic (Figure 3). A comparison between the downscaled values from the NCEP data and the actual data, and the estimates for $R^2 \in [0.82, 9, 97]$ and a p-value ~ 0 from analysis of variance (ANOVA) suggest that the downscaling models capture most of the variations in the January temperature at these locations. Figure 3 shows the geographical distribution of temperature anomalies associated with temperature variations in Oslo, and the strongest anomalies are seen in the vicinity of Oslo in a good accord with the expectations. The predictors in this case were taken from the region 60°W–40°E and 50°N–74°N. Figures 4–5 show time-series and qq-plots of the residual. There are no clear signs of any structure in the residuals and the residuals are close to being normally distributed. Hence, we may have some confidence in these downscaling models.

The trend analysis, shown in Figure 6, shows the long-time tendencies (rate-of change) associated with the best-fit linear and fifth-order polynomial expressions. The linear trend is also shown in Figure 2, suggesting a mean constant warming rate estimated for the period "1960"–"2049" in the range 0.01–0.08°C/decade. The strongest warming is found in Oslo and the weakest warming is found in Helsinki, however, these differences may not be statistically significant.

Figure 7 shows results from an analysis similar to that shown in Figure 2, but where the predictor has been selected from a smaller region (smaller predictor domain: 0°E–40°Eand 55°N–69°N). The geographical distribution of the surface air anomalies associated with the local temperature variations and the six sites are shown in Figure 8. The ANOVA results suggest a better fit: R^2 is in the range 0.92–0.98 and a p-value of zero. The best-fit linear trends suggest warming rates of 0.01–0.10°C/decade, with strongest warming in Stockholm and weakest warming in Tromsø (these differences may not be statistically significant). The warming rates estimated using `clim.pact` are weaker than reported in

*There are also other definitions for "daily mean", e.g. 07.00–07.00 local time, corresponding to the definition of a "day" in hydrological modelling.

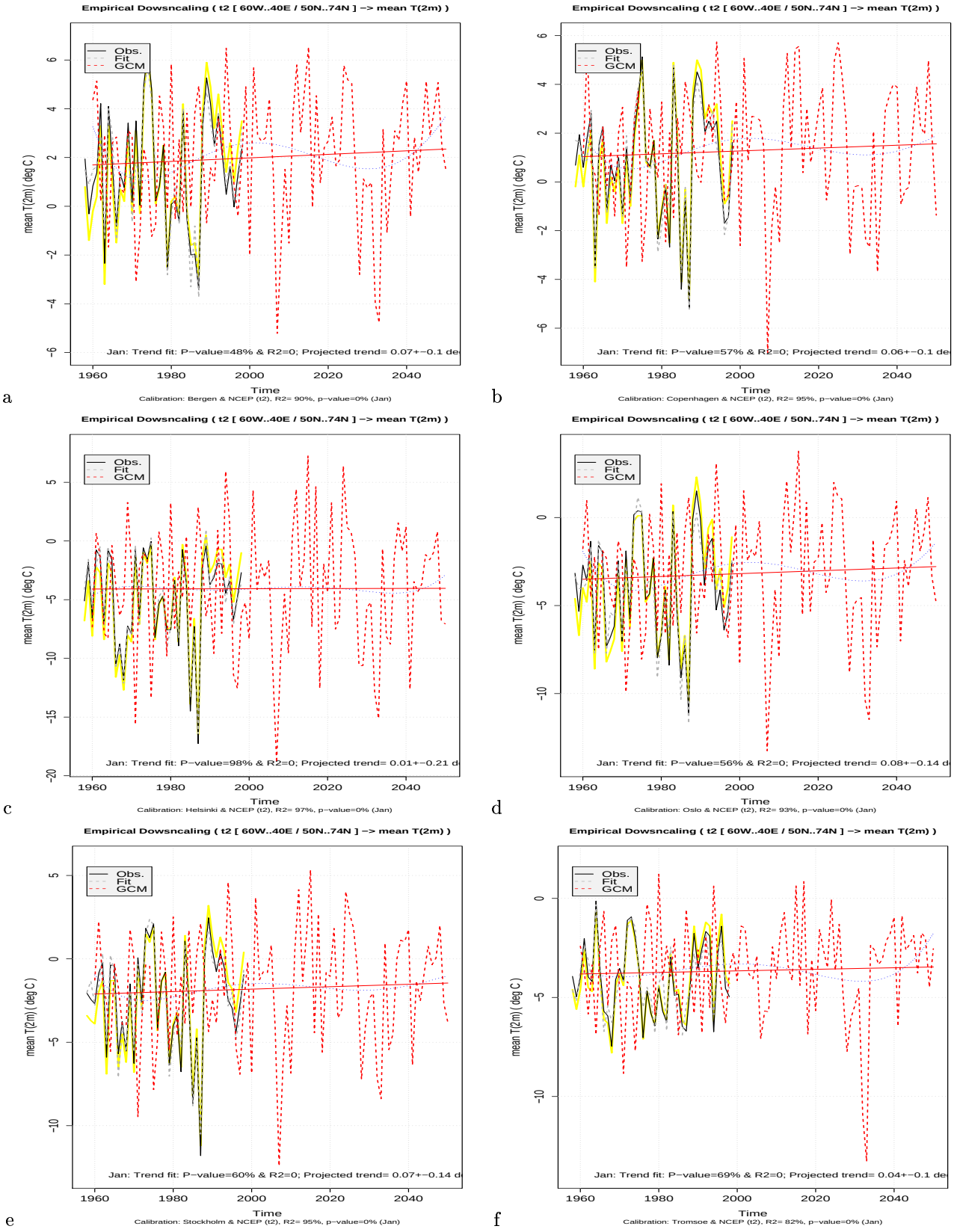

Figure 2. Local January temperature scenarios for Bergen (a), Copenhagen (b), Helsinki (c), Oslo (d), Stockholm (e) and Tromsø (f) produced with the `clim.pact` function `ds()`. The predictor was NCEP T(2m) field covering 60°W–40°Eand 50°N–74°N. The red curves show the downscaled scenario and best-fit linear trend. The observations are shown in black, and the yellow curve shows the original data series before de-trending. The blue curve shows the best-fit 5th-order polynomial trend.

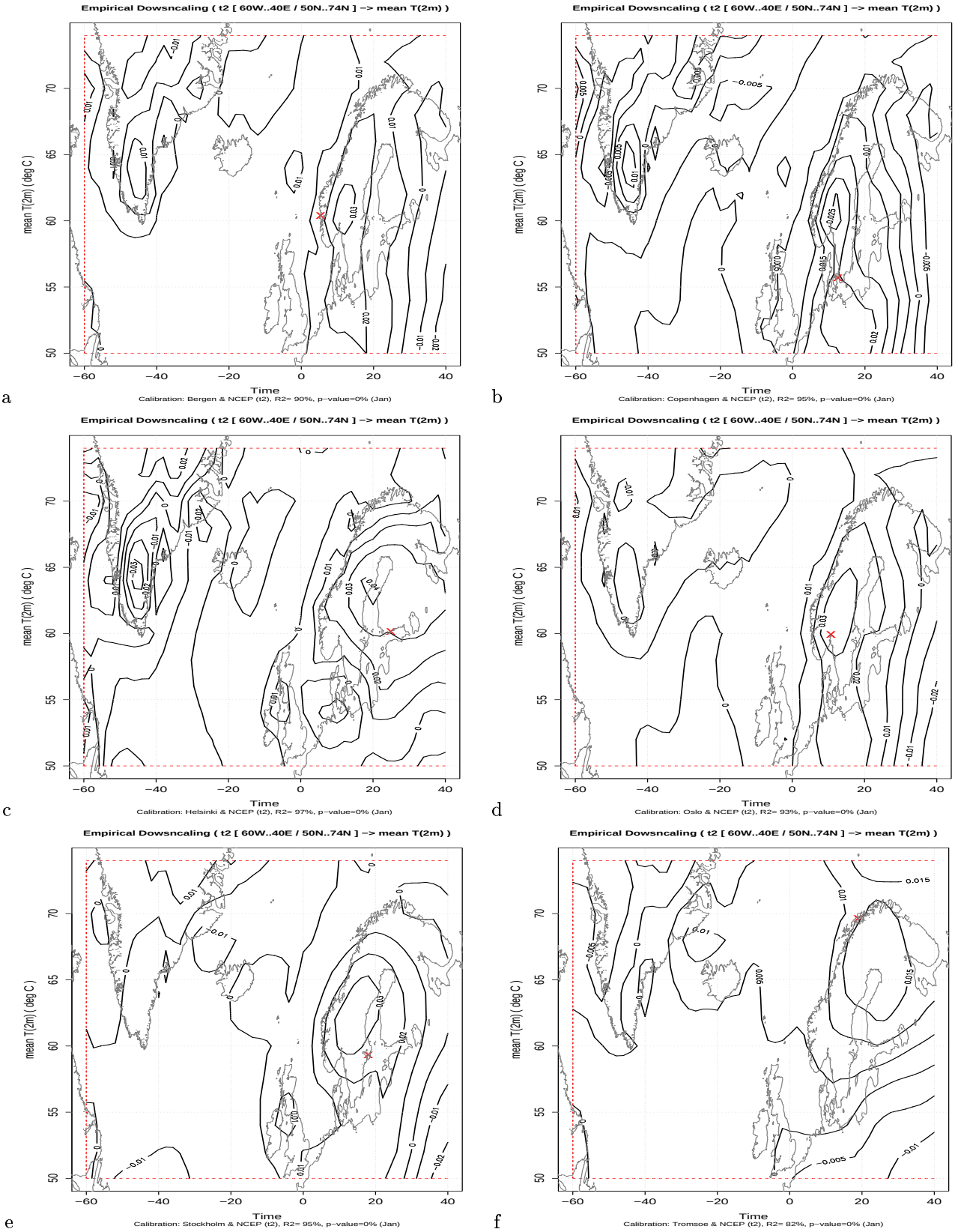

Figure 3. The large-scale spatial temperature anomalies associated with local January temperature variations in Bergen (a), Copenhagen (b), Helsinki (c), Oslo (d), Stockholm (e) and Tromsø (f) produced with the `clim.pact` function `ds()`. The predictor was NCEP T(2m) field covering 60°W–40°E and 50°N–74°N.

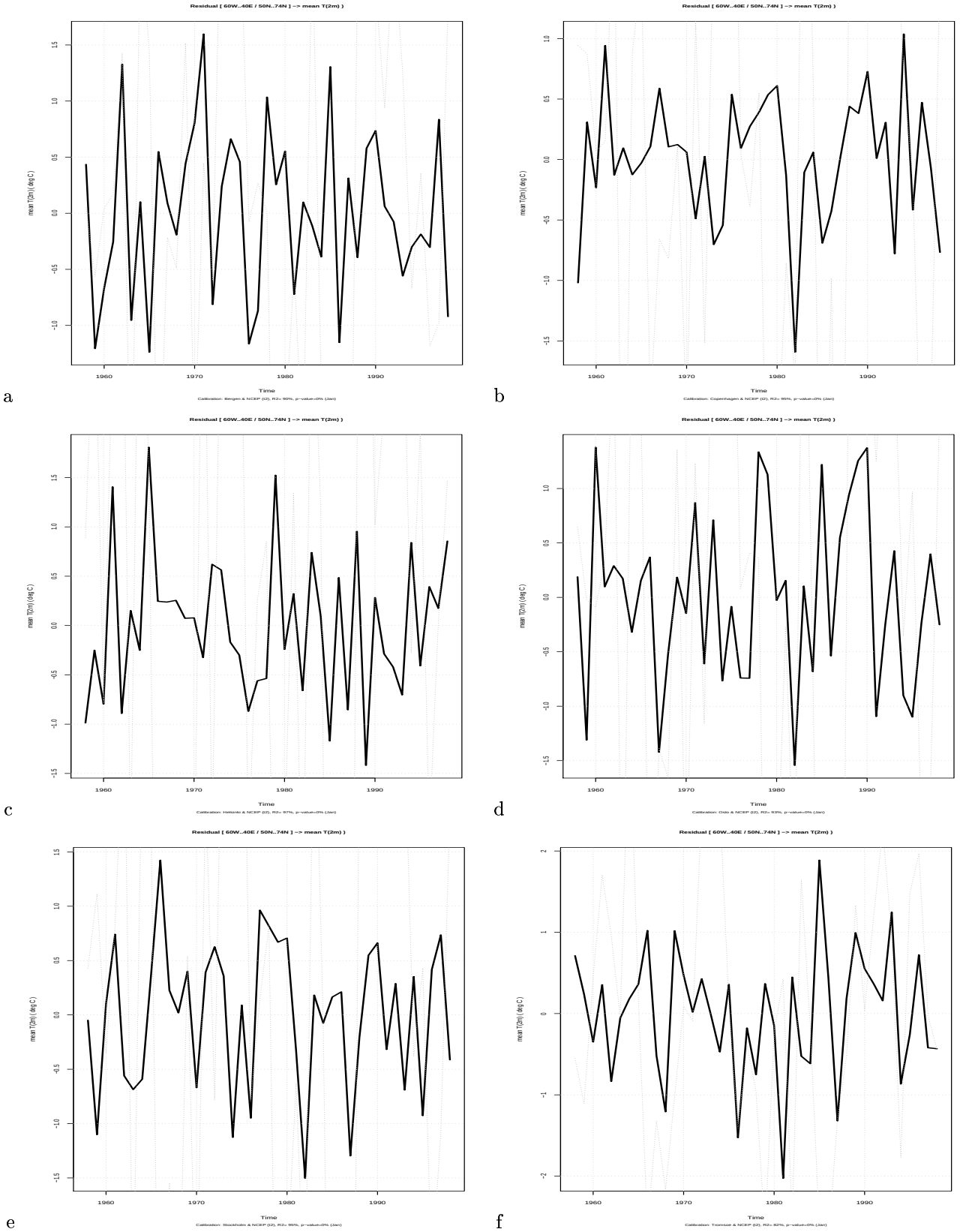

Figure 4. Residuals (black) associated with local January temperature scenarios for Bergen (a), Copenhagen (b), Helsinki (c), Oslo (d), Stockholm (e) and Tromsø (f) produced with the `clim.pact` function `ds()`. The predictor was NCEP T(2m) field covering 60°W–40°Eand 50°N–74°N. The actual values are shown in grey.

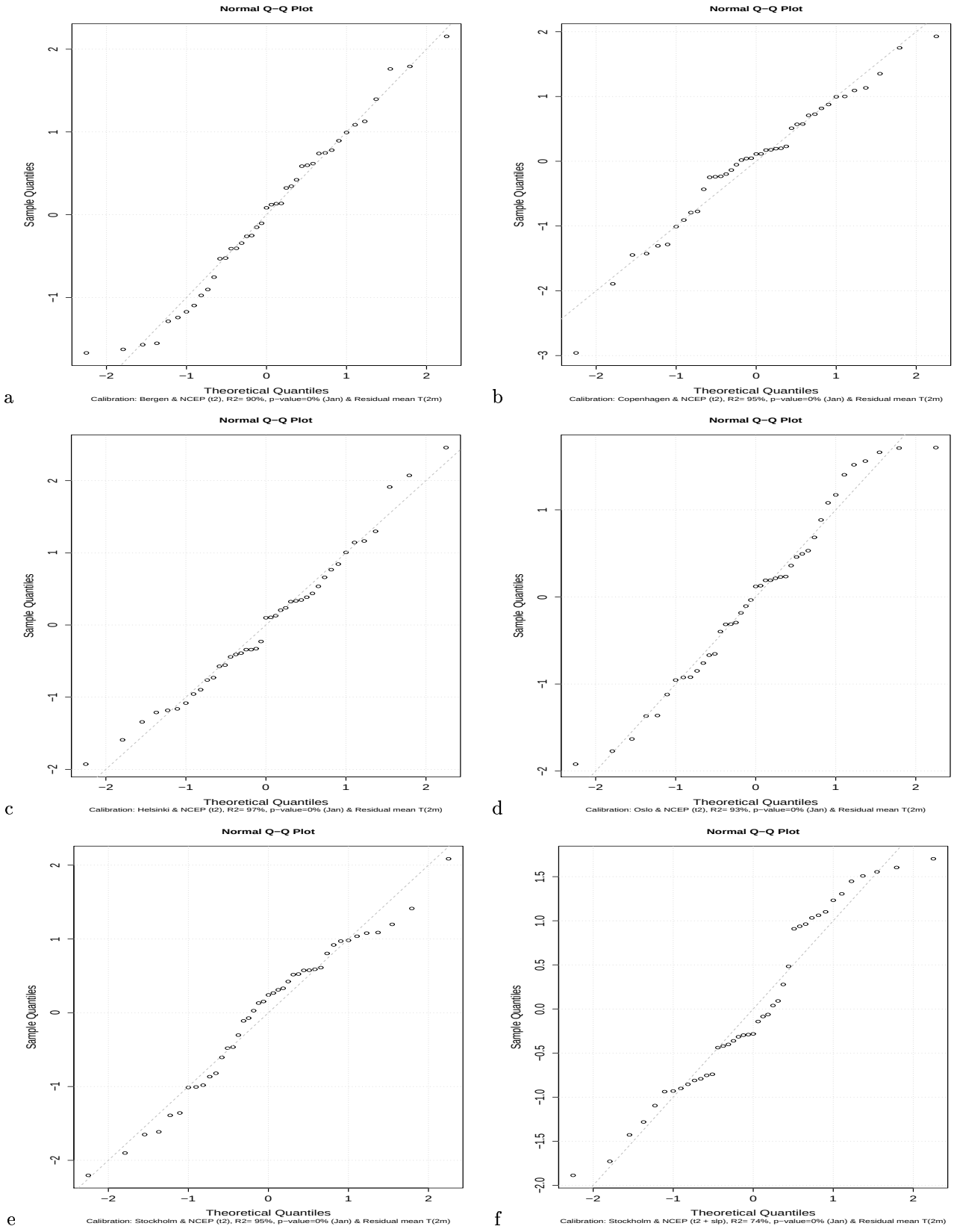

Figure 5. QQ-plots of residuals associated with local January temperature scenarios for Bergen (a), Copenhagen (b), Helsinki (c), Oslo (d), Stockholm (e) and Tromsø (f) produced with the `clim.pact` function `ds()`. The predictor was NCEP T(2m) field covering 60°W–40°Eand 50°N–74°N.

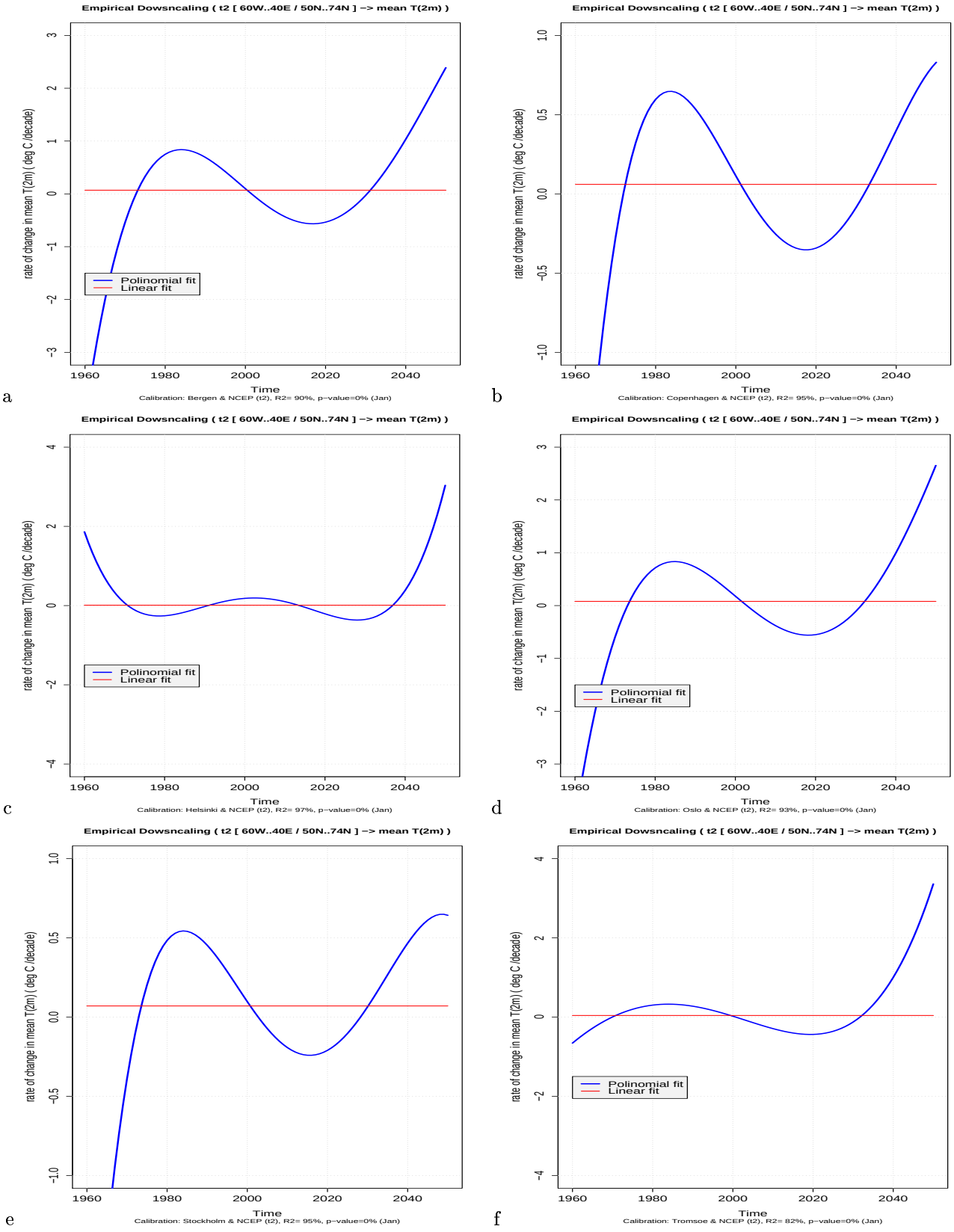

Figure 6. The rate-of-change associated with local January temperature scenarios in Bergen (a), Copenhagen (b), Helsinki (c), Oslo (d), Stockholm (e) and Tromsø (f) produced with the `clim.pact` function `ds()`. The predictor was NCEP T(2m) field covering 60°W–40°Eand 50°N–74°N.

earlier studies. *Benestad* (2000b) downscaled the ECHAM4/OPYC3 GSDIO scenario using an empirical approach involving common EOFs and canonical correlation analysis (CCA) and estimated warming rates for Oslo in the range 0.18–0.63°C/decade for the "1980"–"2049" interval (as opposed to "1960"–"2049" in the `clim.pact` results). This analysis was based on 1873–1998 reconstructed temperatures described by *Benestad* (2000a) as opposed to NCEP re-analysis, and the study by *Benestad* (2000b) utilised a cross-validation analysis based on correlation to select the predictors whereas `clim.pact` uses an `R`-function for step-wise screening. The analysis based on `clim.pact` appears to account for more of the local temperature since the *Benestad* (2000b) study (correlation of 0.70–0.79) implies R^2 estimates in the range 0.49–0.62. The difference between the previous study and the results here can also be found in the maps showing the geographical distribution of temperature anomalies associated with the January temperature in Oslo. In *Benestad* (2000b) (Figure 22d), the strongest anomalies are found over Finland, whereas `clim.pact` finds the strongest anomalies in southern Norway (Figure 3). The differences between these two maps are furthermore consistent with the higher R^2 values obtained with the `clim.pact` code, since the correlation is expected to drop with distance from the predictand location. One explanation for the different results is that the two analyses used different data sets for the observations: the *Benestad* (2000b) results were derived using a temperature reconstruction based on a statistical technique involving the projection of spatial modes derived from gridded observations, and the data is expected to contain errors (*Kaplan* et al., 1998). The NCEP re-analysis, however, is derived from a climate model that assimilates a number of observations, and these results suggest that the NCEP data do give a good description of the surface air temperature variations over Scandinavia.

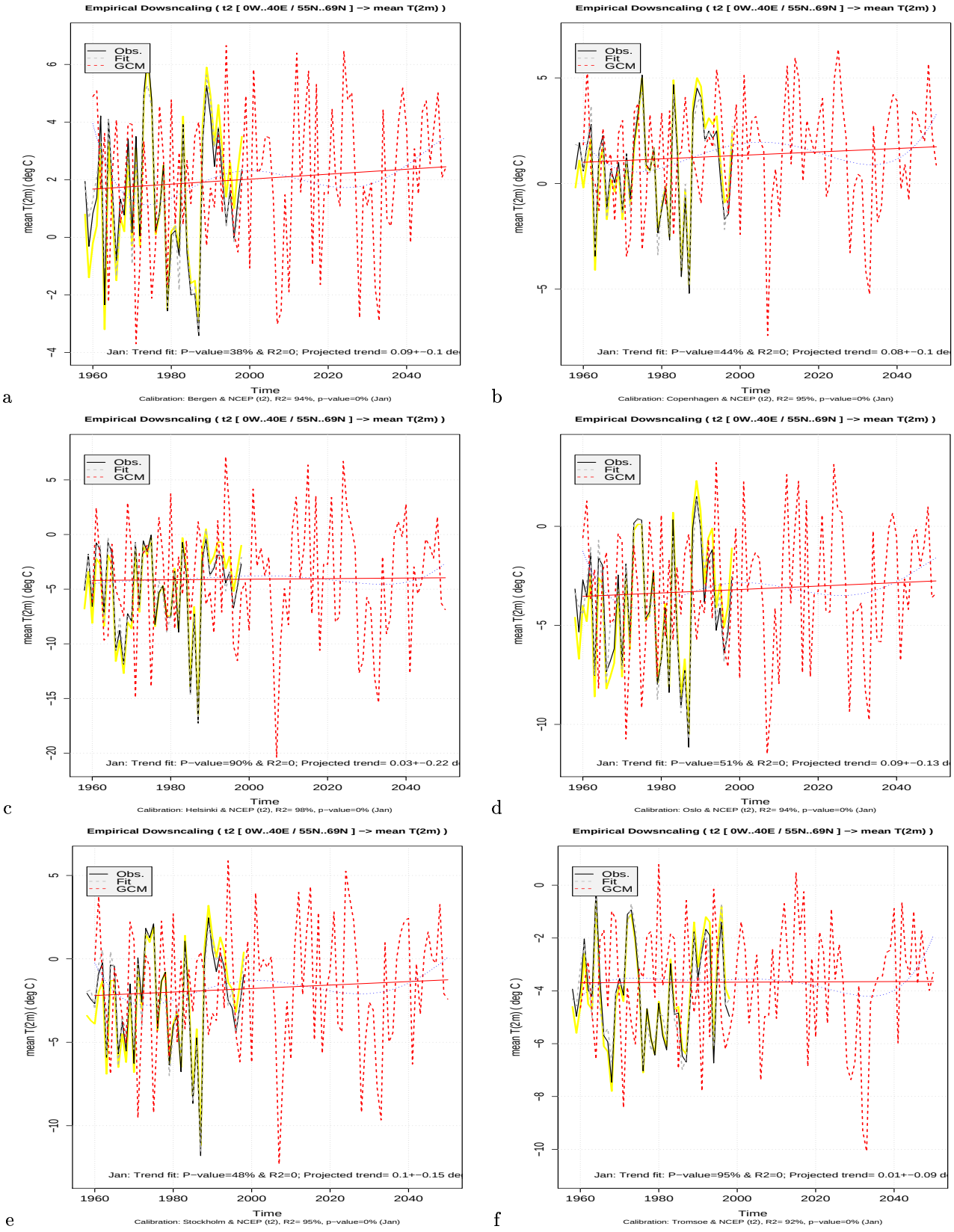

Figure 7. Local January temperature scenarios for Bergen (a), Copenhagen (b), Helsinki (c), Oslo (d), Stockholm (e) and Tromsø (f) produced with the `clim.pact` function `ds()`. The predictor was NCEP mixed T(2m) and SLP fields covering 0°E–40°Eand 55°N–69°N. The red curves show the downscaled scenario and best-fit linear trend. The observations are shown in black, and the yellow curve shows the original data series before de-trending. The blue curve shows the best-fit 5th-order polynomial trend.

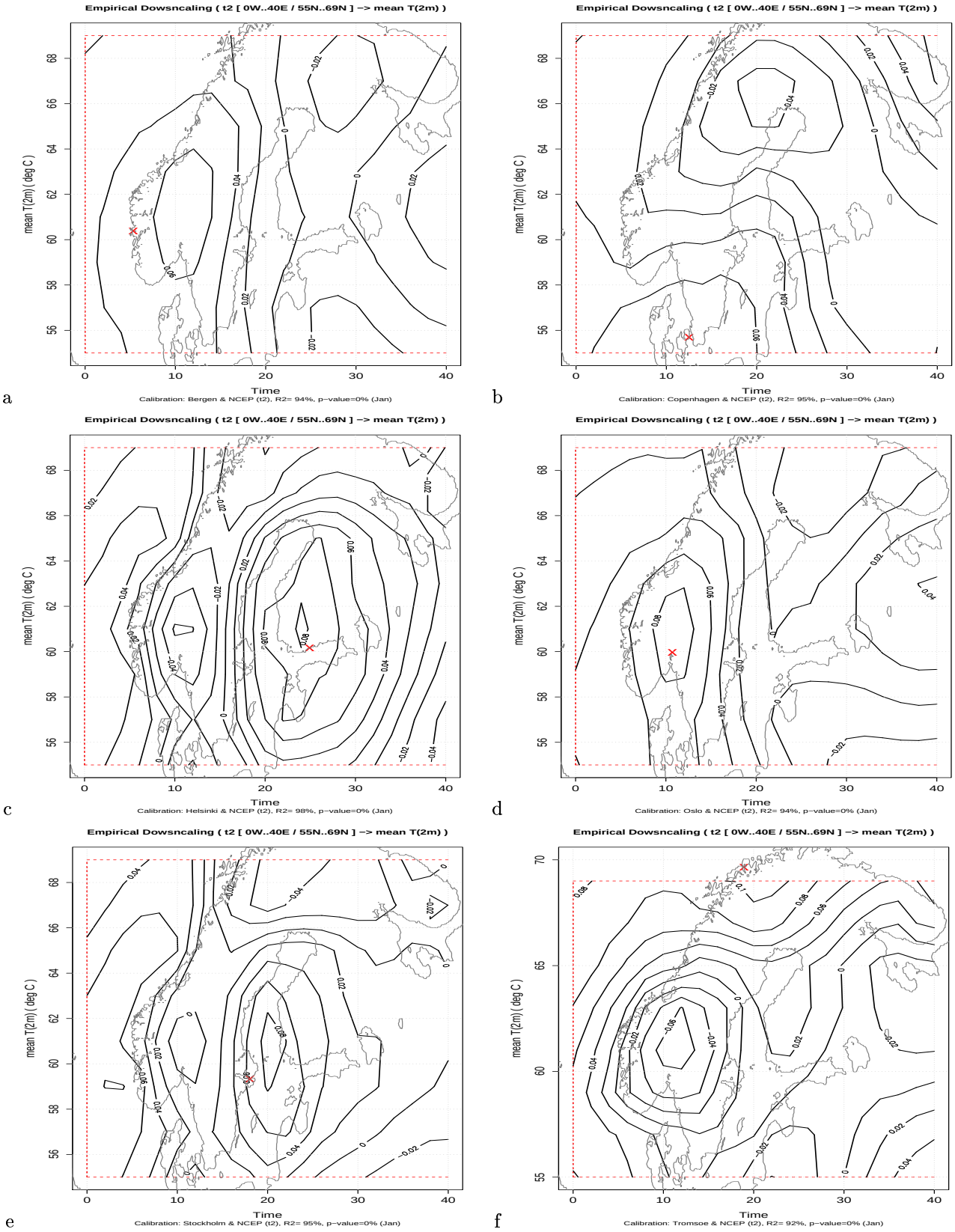

Figure 8. The large-scale spatial temperature anomalies associated with local January temperature variations in Bergen (a), Copenhagen (b), Helsinki (c), Oslo (d), Stockholm (e) and Tromsø (f) produced with the `clim.pact` function `ds()`. The predictor was NCEP mixed T(2m) and SLP fields covering 0°E–40°Eand 55°N–69°N. The red curves show the downscaled scenario and best-fit linear trend. The observations are shown in black, and the yellow curve shows the original data series before de-trending. The blue curve shows the best-fit 5th-order polynomial trend.

3.1.2 Differences due to single and mixed fields

The empirical downscaling may also use a combination of several climate elements as predictors. Figures 9–12 show the results of analyses corresponding to those shown in Figures 2–8, based on mixed-common EOF predictors. In this case, a combination of surface air temperature and sea level pressure have been used as predictors. Figures 13–14 show the residuals for a selection of locations. The residuals and the ANOVA results for the analysis derived with predictors from 60°W–40°Eand 50°N–74°N (Figures 9 and 11) suggest that there is a strong relationship between the coupled field and the local temperature (R^2 is 0.74–0.78, p-value $\sim$ 0), albeit slightly weaker than when only temperature is used as predictor. The estimated warming rates corresponding to the best-fit linear trends are 0.15–0.61°C/decade, with weakest warming in Tromsø and strongest in Helsinki. It is interesting to note that the mixed-field common EOFs produce substantially stronger warming than the common EOFs consisting of temperature only. With the mixed-field common EOFs, the linear trend for Oslo suggests a warming of 0.54°C/decade, which is in good agreement with the results in *Benestad* (2000b).

Figure 10 shows the geographical distribution of coupled temperature (black) and SLP (blue) anomalies associated with the local temperature variations. The most striking feature is seen over Greenland, where the temperature anomalies are negative and the pressure is high. This pattern is similar for the climate stations in southern Fennoscandia, but January Tromsø temperature as a stronger relationship with anomalous westerly geostrophic winds and the temperature over northern Finland and the Kola peninsula.

The downscaling analysis was repeated using a smaller predictor domain (0°W–40°Eand 55°N–69°N), and the statistical relationship between large and small scales was strengthened by the omission of the North Atlantic (R^2 is 0.81–0.96, p-value $\sim$ 0). The results are shown in Figures 11–12. The maps in Figure 12 suggest that a warm January in Bergen, Copenhagen, or Oslo tends to be associated with anomalous southerly winds, high pressure over eastern Norway and parts of Sweden, and cold conditions over northern Finland. The January temperature in Helsinki and Tromsø, on the other hand, is correlated with the temperature in northern Finland, and the Helsinki temperature is furthermore associated with local low pressure. The January temperature in Stockholm is associated with local low pressure in conjunction with warm conditions over the southern Baltics.

The warming rates derived using a smaller predictor domain are in the range 0.26–0.87°C/decade. Again, the weakest January warming is found in Tromsø and the strongest warming is seen in Helsinki. The warming rate for Oslo was estimated to be 0.54°C/decade. Hence, these results are in good agreement with the estimates in *Benestad* (2000b).

Figures 13–14 show analyses of the residuals from the regression (model calibration) analysis. There is no evidence of structure in these plots and the residuals appear to be approximately normally distributed without any bias.

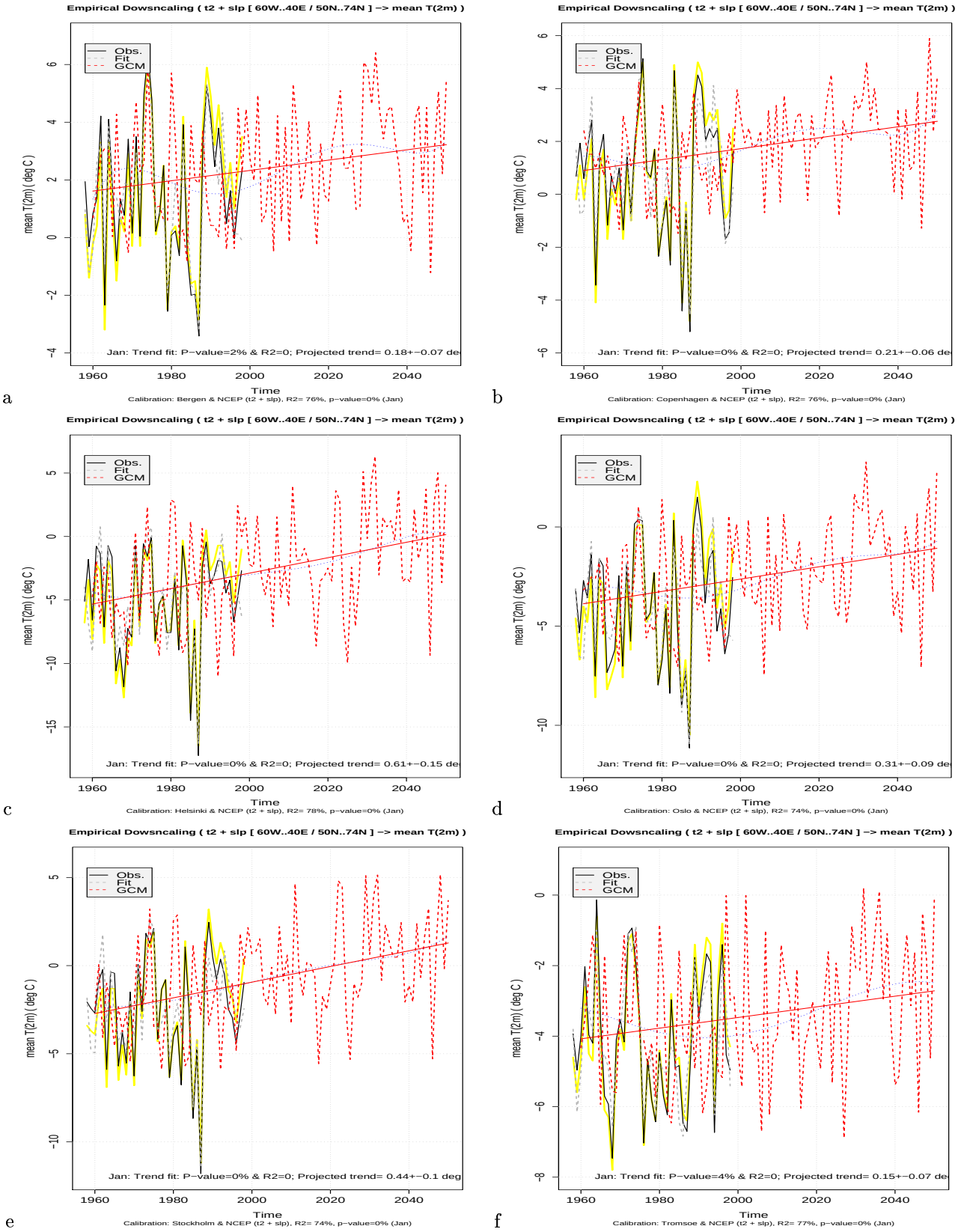

Figure 9. Local January temperature scenarios for Bergen (a), Copenhagen (b), Helsinki (c), Oslo (d), Stockholm (e) and Tromsø (f) produced with the `clim.pact` function `ds()`. The predictor was NCEP combined T(2m) and SLP fields covering 60°W–40°Eand 50°N–74°N. The red curves show the downscaled scenario and best-fit linear trend. The observations are shown in black, and the yellow curve shows the original data series before de-trending. The blue curve shows the best-fit 5th-order polynomial trend.

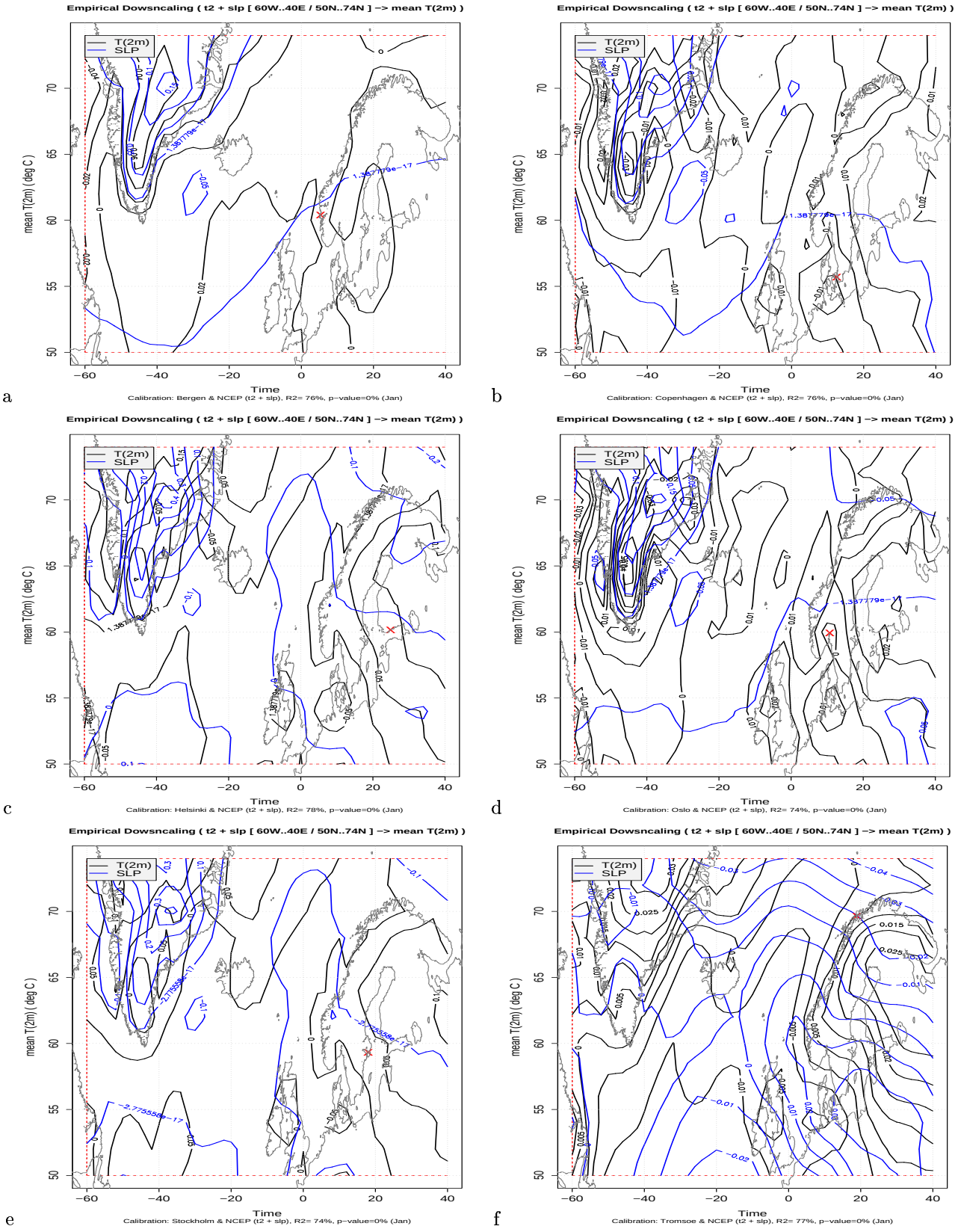

Figure 10. The large-scale spatial temperature anomalies associated with local January temperature variations in Bergen (a), Copenhagen (b), Helsinki (c), Oslo (d), Stockholm (e) and Tromsø (f) produced with the `clim.pact` function `ds()`. The predictor was NCEP combined T(2m) and SLP fields covering 60°W–40°Eand 50°N–74°N.

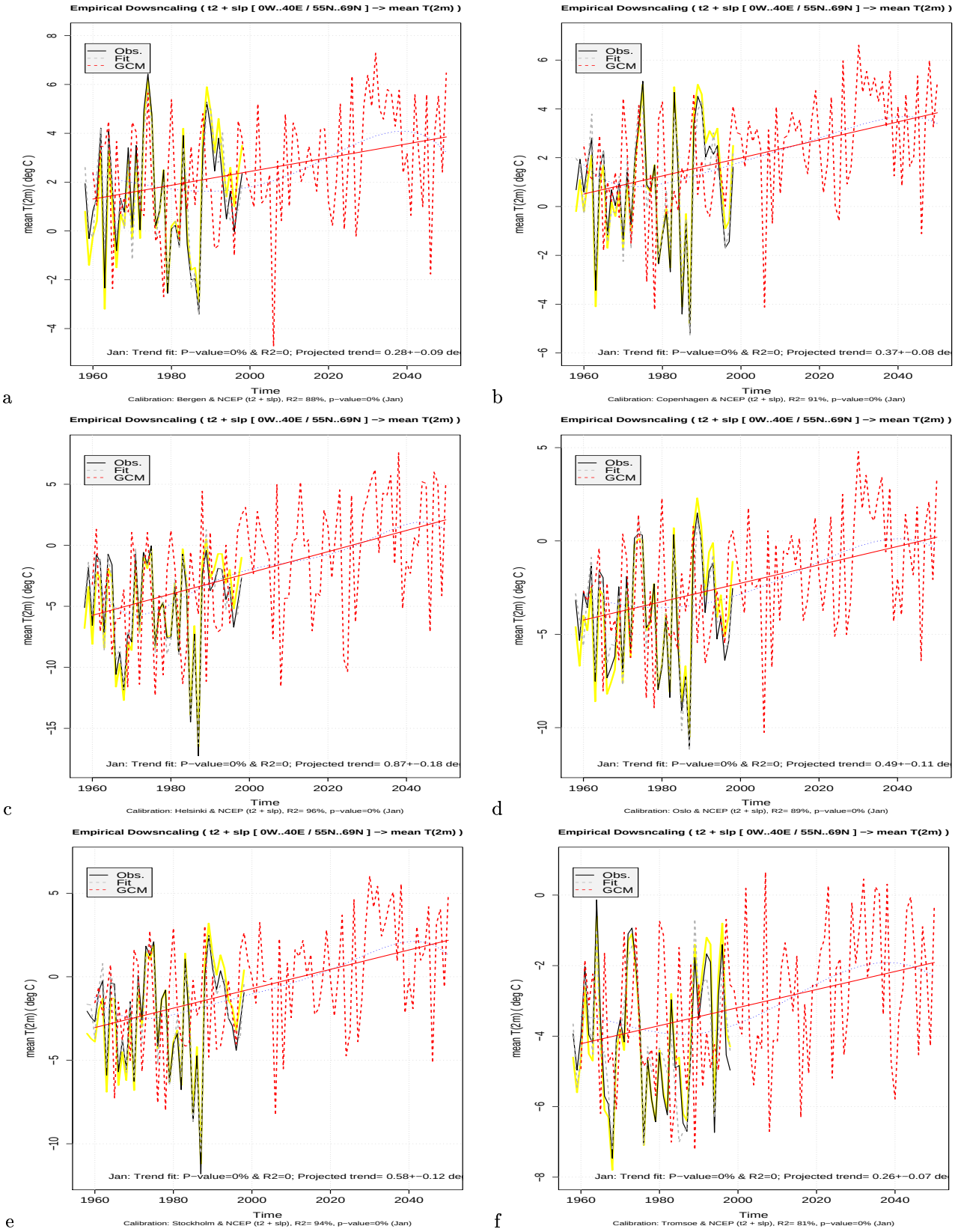

Figure 11. Local January temperature scenarios for Bergen (a), Copenhagen (b), Helsinki (c), Oslo (d), Stockholm (e) and Tromsø (f) produced with the `clim.pact` function **`ds()`**. The predictor was NCEP mixed T(2m) and SLP fields covering 0°E–40°Eand 55°N–69°N. The red curves show the downscaled scenario and best-fit linear trend. The observations are shown in black, and the yellow curve shows the original data series before de-trending. The blue curve shows the best-fit 5th-order polynomial trend.

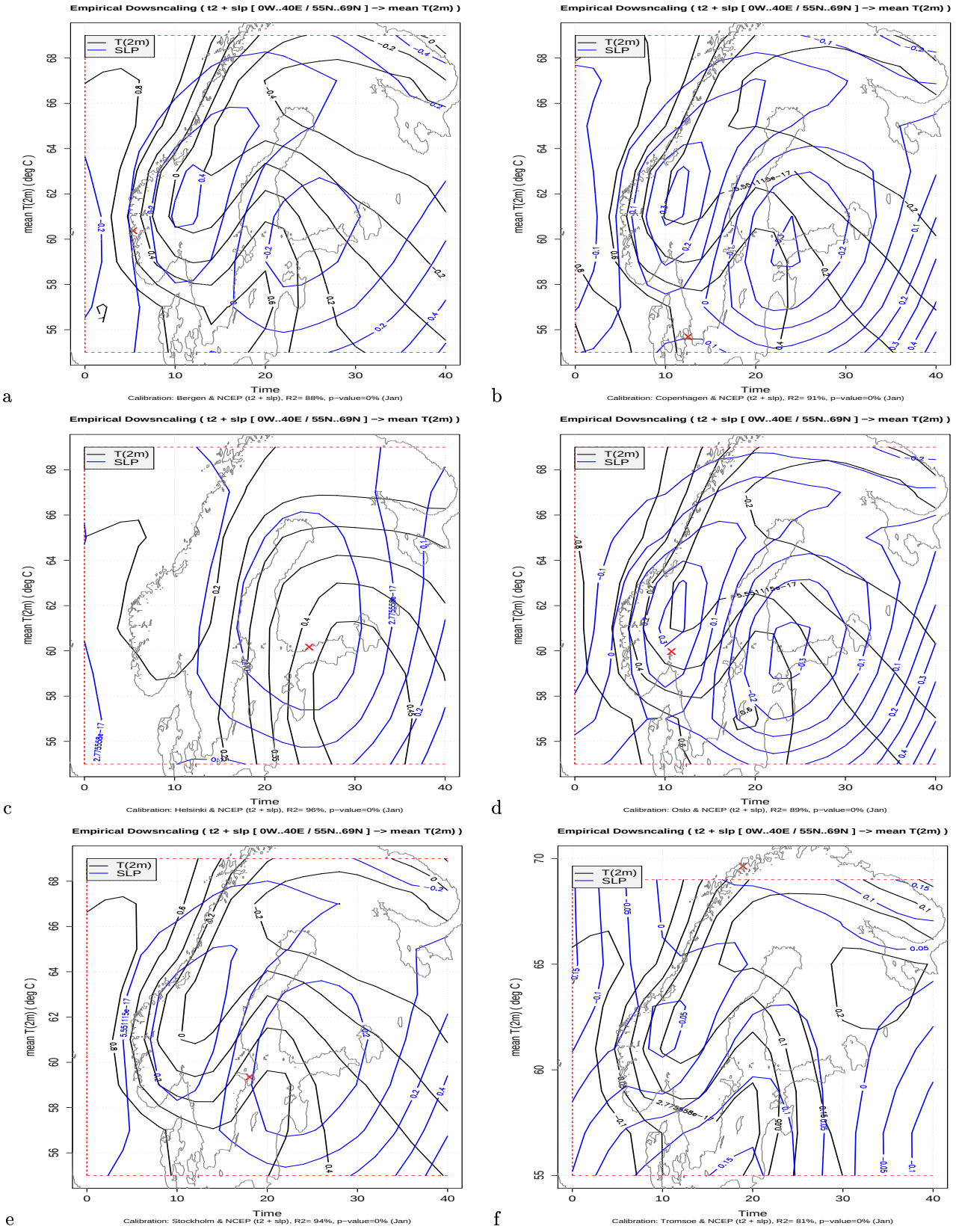

Figure 12. The large-scale spatial temperature anomalies associated with local January temperature variations in Bergen (a), Copenhagen (b), Helsinki (c), Oslo (d), Stockholm (e) and Tromsø (f) produced with the `clim.pact` function **`ds()`**. The predictor was NCEP mixed T(2m) and SLP fields covering 0°E–40°Eand 55°N–69°N.

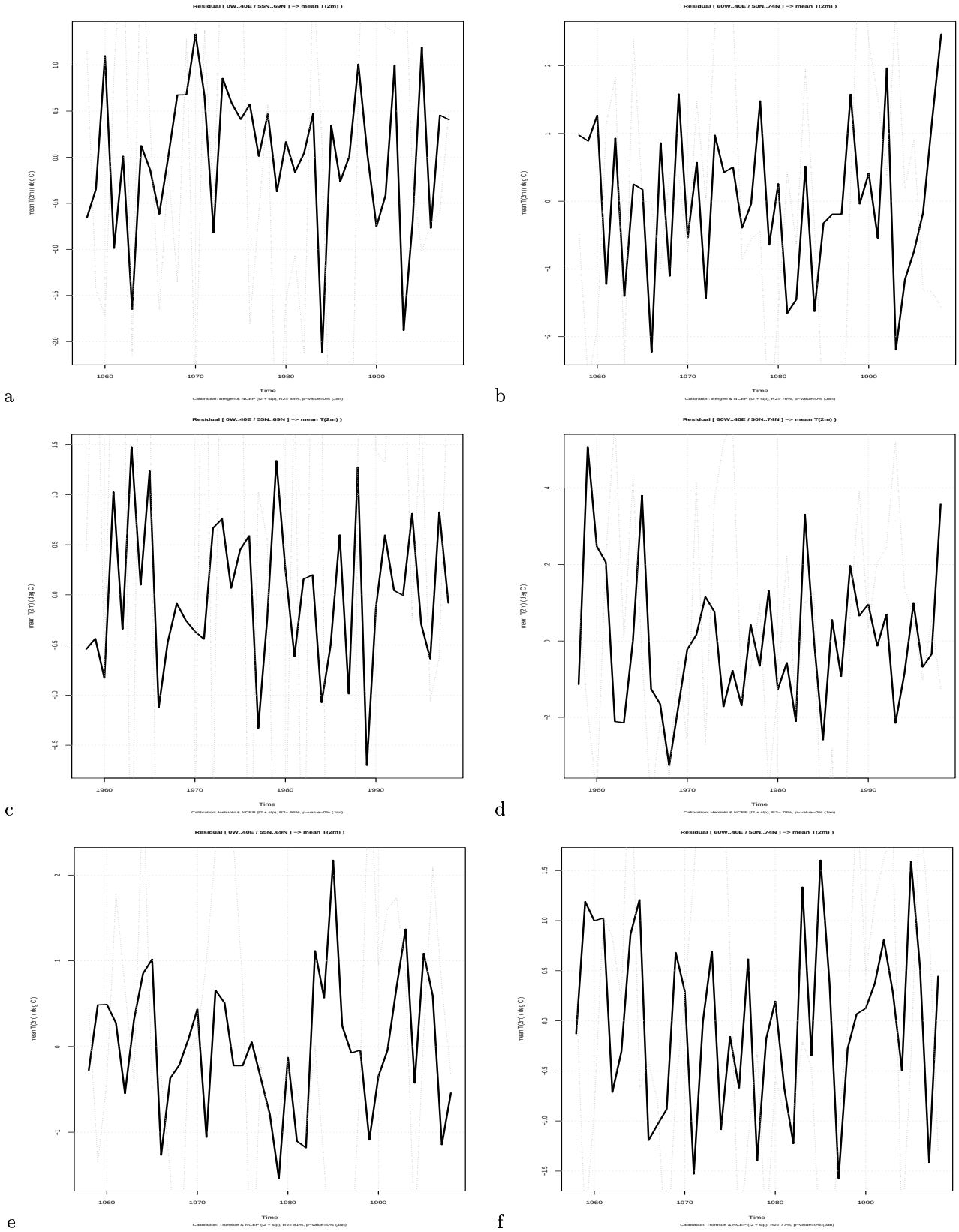

Figure 13. QQ-plots of residuals associated with local January temperature scenarios for Bergen (a,b), Helsinki (c,d) and Tromsø (e,f) produced with the `clim.pact` function `ds()`. The predictor was NCEP combination T(2m) and SLP field covering 60°W–40°E& 50°N–74°Nand 60°W–40°E&50°N–74°N.

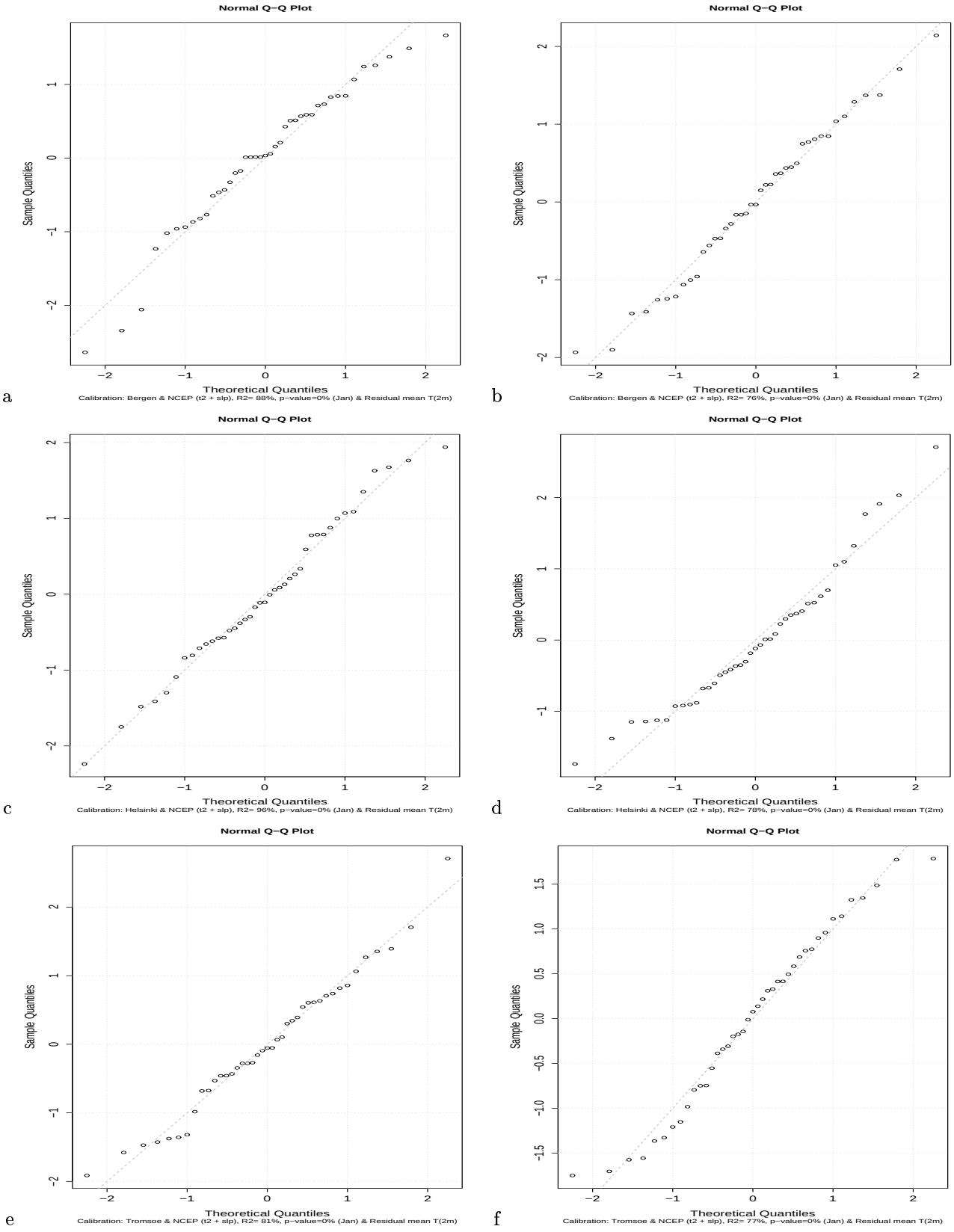

Figure 14. QQ-plots of residuals associated with local January temperature scenarios for Bergen (a,b), Helsinki (c,d) and Tromsø (e,f) produced with the `clim.pact` function `ds()`. The predictor was NCEP combination T(2m) and SLP field covering 60°W–40°E& 50°N–74°Nand 60°W–40°E&50°N–74°N.

3.2 Monthly precipitation

Figure 15 shows the result of the downscaling applied to the January precipitation at Bjørnholt (Nordmarka, just north of Oslo). Panels (a–b) show the time series and distribution of the historical observations. The large interannual variations make the detection of long-term trends difficult.

Panels (c–f) show the results from the downscaling. The ANOVA results indicate a strong and good relationship between local January precipitation and large-scale anomalies: $R^2 = 0.64$, p-value ~ 0. Increased precipitation is associated with anomalous southerly flow, and high pressure and low temperatures over Greenland. The linear trend analysis (e) suggests a a weak long-term increase whereas a polynomial trend-fit suggests a dramatic change towards a wetter climate at the end of the scenario (polynomial trends are sensitive to the end points of the series, and hence this acceleration may reflect interannual variations). The residual of the regression analysis (f) does not suggest that there is any structure.

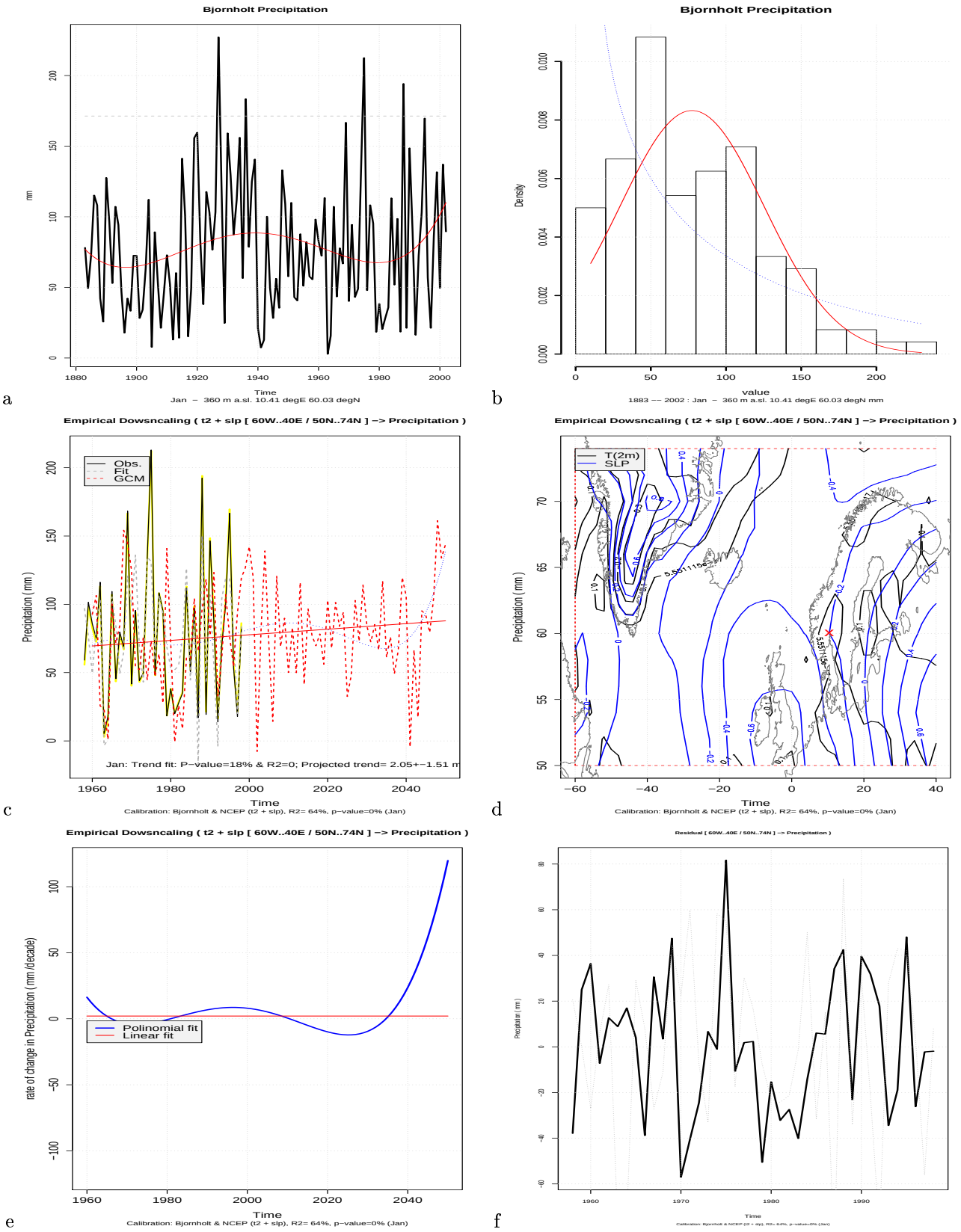

Figure 15. January precipitation scenarios for Bjørnholt produced with the `clim.pact` functions `plot.nordklim()` (a,b) and `ds()` (c–f). The predictor was NCEP combined T(2m) and SLP fields covering 60°E–40°Eand 50°N–74°N. (a) Observed time series; (b) histogram of snow-depths with Gaussian (red) and Gamma (blue) distribution superimposed; (c) downscaled precipitation scenario; (d) spatial large-scale coupled January T(2m)-SLP pattern associated with contemporary precipitation; (e) rate of change of January precipitation; (f) time series of residual from the regression (calibration of downscaling model).

3.3 Monthly mean snow-depth

The downscaling may easily be extended to any record that has a statistically valid relationship with large-scale climatic anomalies. In Figure 16, the downscaling has been carried out for the January mean snow-depth at Cuouddatmohkki in Finnmark county (96.22°N, 24.26°E). The observations suggests that there have been two January months with "extreme"* snow-depths greater than 50 cm at Cuouddatmohkki. This snow-depth record is unfortunately too short to make any firm statement about long-term trends, and the number of observations is too small to get a good histogram describing the distribution of values (b). The brief record also makes the empirical model calibration uncertain, but R^2 estimates of 0.29–0.31 suggests that there may be a relationship between the snow-depth and the coupled T(2m)-SLP pattern. However, a p-value of 0.09 suggests that this relationship is not statistically significant at the 5% level. The geographical distribution of T(2m) and SLP anomalies in panel (d) associates the snow-depth with anomalous westerly geostrophic winds and low temperatures, which physically plausible. It is also important to realize that the January snow-depth also is affected by the November–December snow-fall, and the downscaling could possibly be improved by repeating the analysis with predictor fields derived from November–January T(2m) and SLP.

It is nevertheless interesting to note that the downscaled scenarios for the snow-depth at Cuouddatmohkki points to a trend of more snow, both when using predictors from 0°E–40°Eand 55°N–69°N as well as 60°W–40°Eand 50°N–74°N. An inspection of the residuals (e) suggests that there is no structure (the record is possibly too short to see any structure anyway), and that $\sim \frac{1}{3}$ of the snow-depth in 1980 could accounted for by this analysis.

*Here "extreme" is defined in terms of the 1970–2000 period.

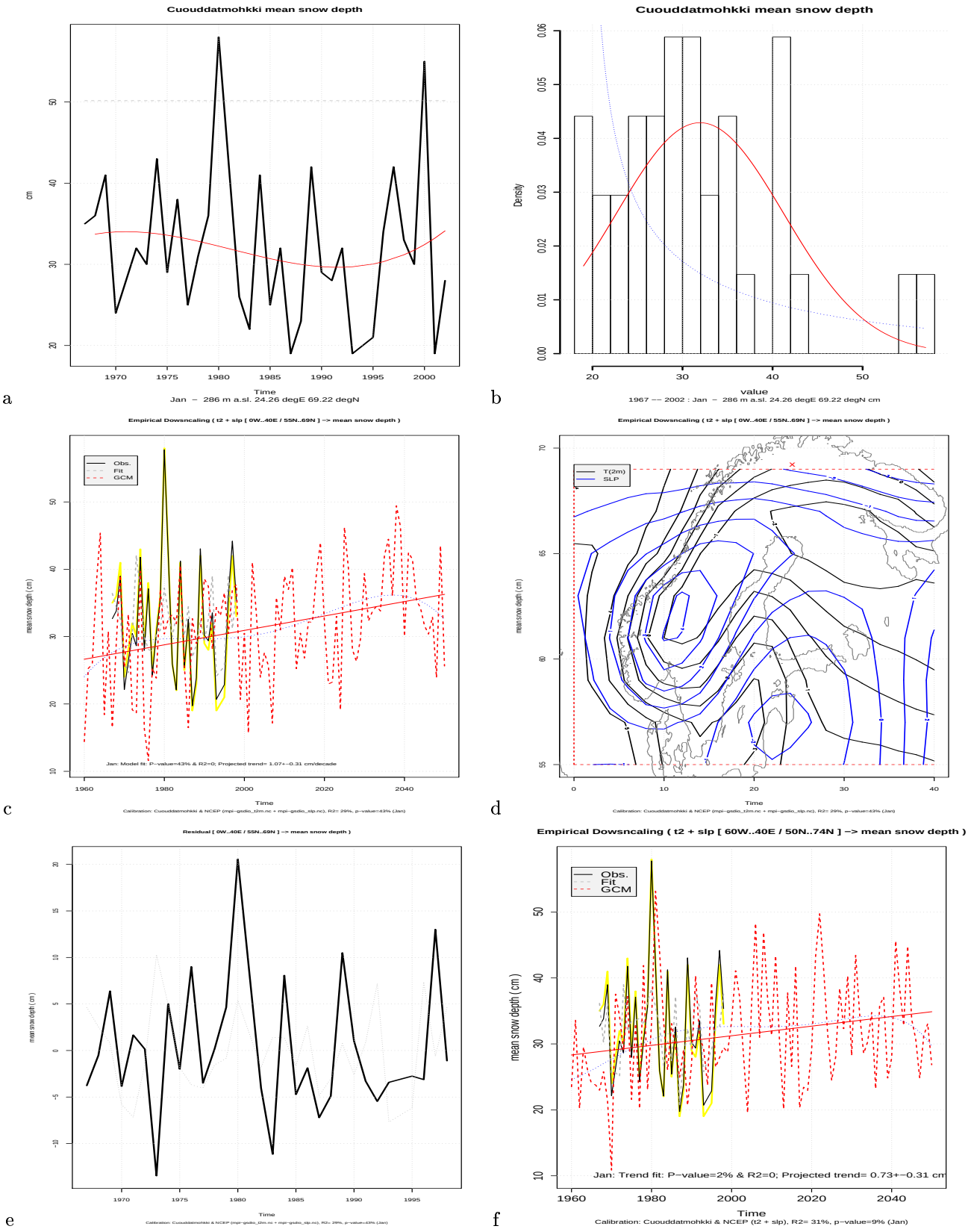

Figure 16. Local January snow-depth observations scenarios for Cuouddatmohkki produced with the `clim.pact` functions `plot.nordklim()` (a,b) and `ds()` (c–f). The predictor was NCEP combined T(2m) and SLP fields covering 0°E–40°Eand 55°N–69°N. (a) Observed time series; (b) histogram of snow-depths with Gaussian (red) and Gamma (blue) distribution superimposed; (c) downscaled snow-depth scenario; (d) spatial large-scale coupled Jannuary T(2m)-SLP pattern associated with contemporary snow-depth; (e) time series of residual from the regression (calibration of downscaling model); (f) downscaled snow-depth scenario using a predictor covering 60°W–40°Eand 50°N–74°N.

3.4 Daily mean temperature

3.5 Downscaling using sea-level pressure as predictor fields

The daily mean temperature in Oslo and Bergen is approximately Gaussian. According to the qq-plots (Figure 17 and 18, panel (a)), the temperatures are nearly normally distributed near the centre of the distribution, but observed values tend to be greater near the tails than expected if the series were perfectly Gaussian (fat-tail distributed). The fat tails in observations indicate that the extreme value statistics should not be deduced from a Gaussian distribution and that a GEV may be more appropriate.

There is a relationship between the SLP and the daily winter temperature in Oslo and Bergen (panel (b,c)): $R^2 = 0.48$, 0.50 for Oslo and Bergen respectively; p-value ~ 0. A high temperature in Oslo is associated with local low pressure (d), and a physical explanation for this relationship is that low pressure is associated with cloud cover, which subsequently affects the radiation budget in terms of increased trapping of long-wave radiation. Bergen is situated outside the region from which the predictors were picked, and hence the downscaling analysis could probably be improved by repeating the analysis with a region shifted westward by approximately 20 degrees. Figures 17 and 18 show the downscaled results for a control period ("1980"–"199" and "2030"–"2049"), and there is only a marginally small increase in the mean temperature between these two time slices (c,e). There is also a slight hint of increased variance in the "2030"–"2049" time-slice (e). The return value analysis (f) suggests that there may be an increase in the frequency of extreme warm winter days.

It is important to note that there is not a complete overlap between the predictand and predictor in this case: the former represents 06.00-06.00 UTC whereas the latter describes 00.00-00.00 UTC, and there are 6 hours that do not overlap in both data sets. However, due to the persistence in temperature, this time difference is not thought to be a big problem in this case.

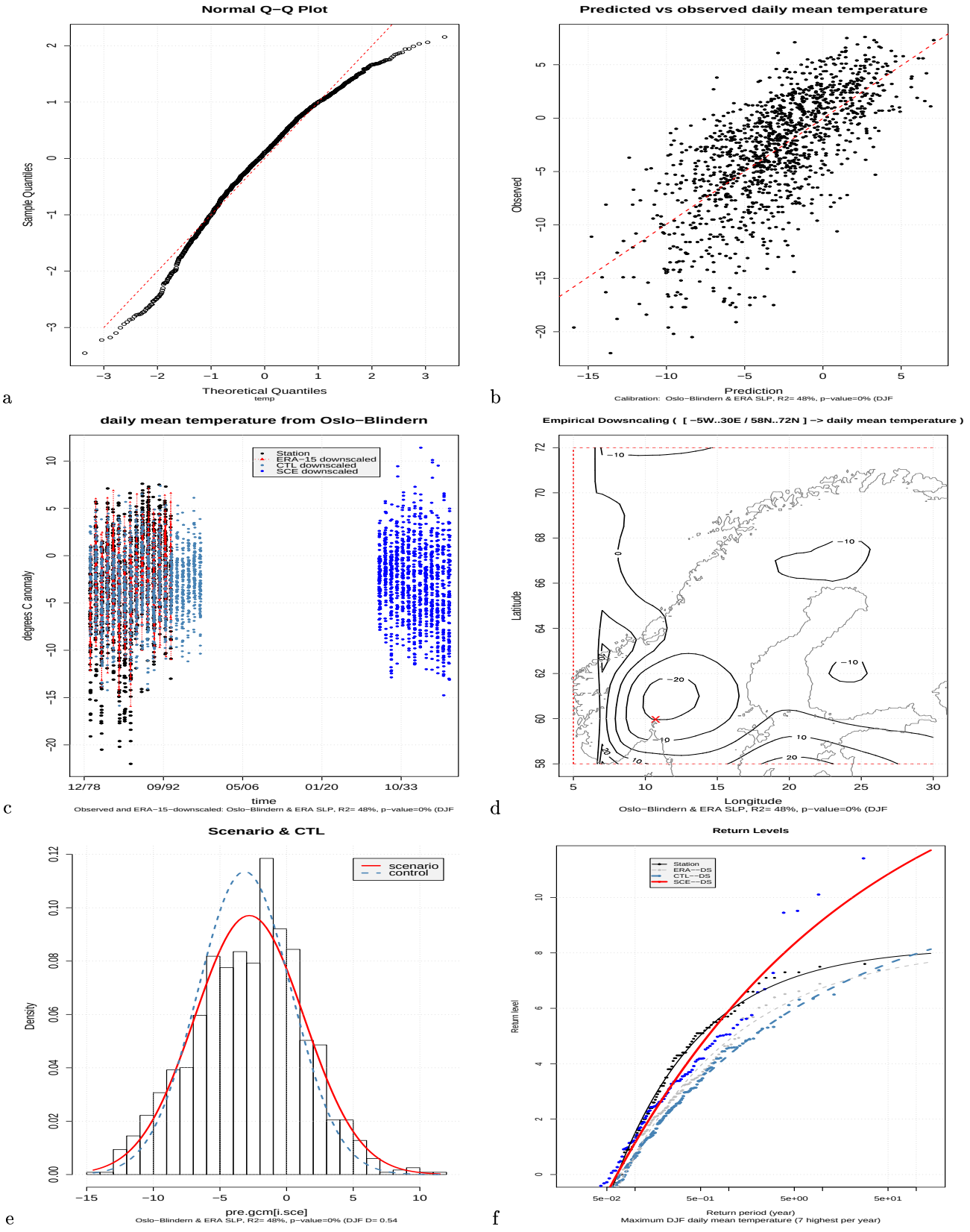

Figure 17. Downscaled results for daily mean winter temperature at Oslo-Blindern. (a) qq-plot of the temperature series, (b) scatter plot between observations and (dependent) predictions, (c) the downscaled values, (d) geographical distribution of T(2m)-SLP field associated with temperature variations in Oslo, (e) comparison between temperature distributions in the control period and scenario, and (f) return-value analysis for daily mean winter temperature in Oslo.

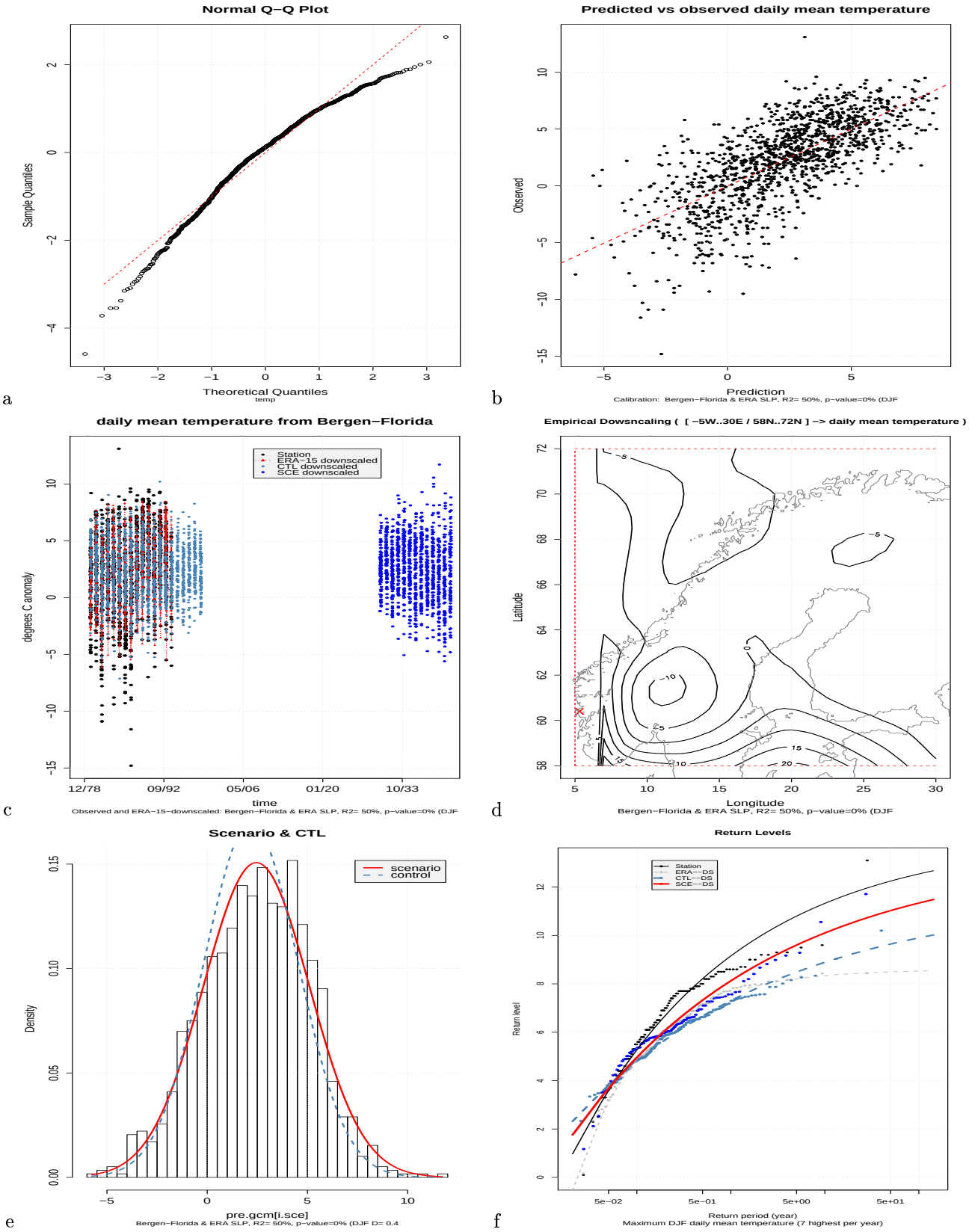

Figure 18. Downscaled results for daily mean winter temperature at Bergen-Florida. (a) qq-plot of the temperature series, (b) scatter plot between observations and (dependent) predictions, (c) the downscaled values, (d) geographical distribution of T(2m)-SLP field associated with temperature variations in Bergen, (e) comparison between temperature distributions in the control period and scenario, and (f) return-value analysis for daily mean winter temperature in Bergen.

3.6 Daily precipitation

The results for the downscaling of daily precipitation in Oslo and Bergen are shown Figures 23 and 24. The precipitation data have been subject to a log-transform, but panel (a) suggests that even after this transform, the data are not normally distributed (no transform results in a worse result). The cluster of points near the lower left corner of panel (a) is due to many dry days. The scatter plot (b, showing the results after the transform has been inverted) suggests that the empirical models give a poor description of the daily precipitation, however, the ANOVA R^2 estimates are 0.32 and 0.30 for Oslo and Bergen respectively (p-value ~ 0). The results shown in panel (c) also indicate that the downscaling occasionally produces precipitation amounts that are unrealistically high (the results shown have been inversely transformed). The geographical distribution of SLP anomalies, suggest a connection between the precipitation in Oslo and low pressure situated to immediately the west, in good agreement with the expectations. A comparison between the downscaled results from the control period and future (e) suggests a slight increase in heavy precipitation, and this shift is "confirmed" by the return value analysis in panel (f). However, a comparison between daily downscaled precipitation derived from the ERA-15 SLP and the actual observations suggests that the downscaled results are not realistic.

It is important to note that there is not a complete overlap between the predictand and predictor in this case: the former represents 18.00-18.00 UTC whereas the latter describes 00.00-00.00 UTC, and there are 6 hours that do not overlap in both data sets. It is possible that all of the rainfall recorded has fallen during those 6 hours, and hence, the time shift may be problematic. The solution to this problem is to use predictors estimated over 18.00-18.00 UTC instead of 00.00–00.00.

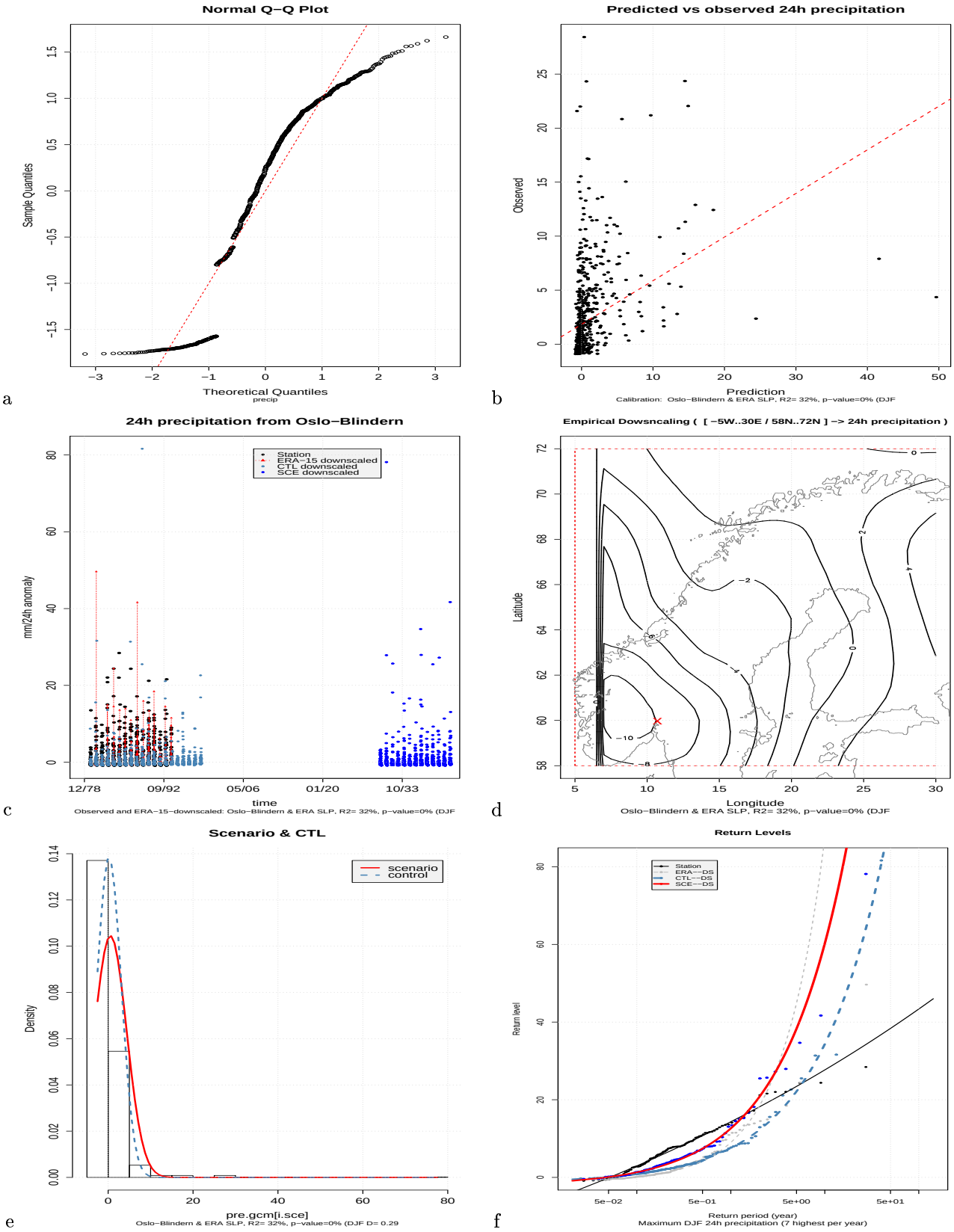

Figure 19. Downscaled results for daily mean winter precipitation at Oslo-Blindern. (a) qq-plot of the precipitation series, (b) scatter plot between observations and (dependent) predictions, (c) the downscaled values, (d) geographical distribution of T(2m)-SLP field associated with precipitation variations in Oslo, (e) comparison between precipitation distributions in the control period and scenario, and (f) return-value analysis for daily mean winter precipitation in Oslo.

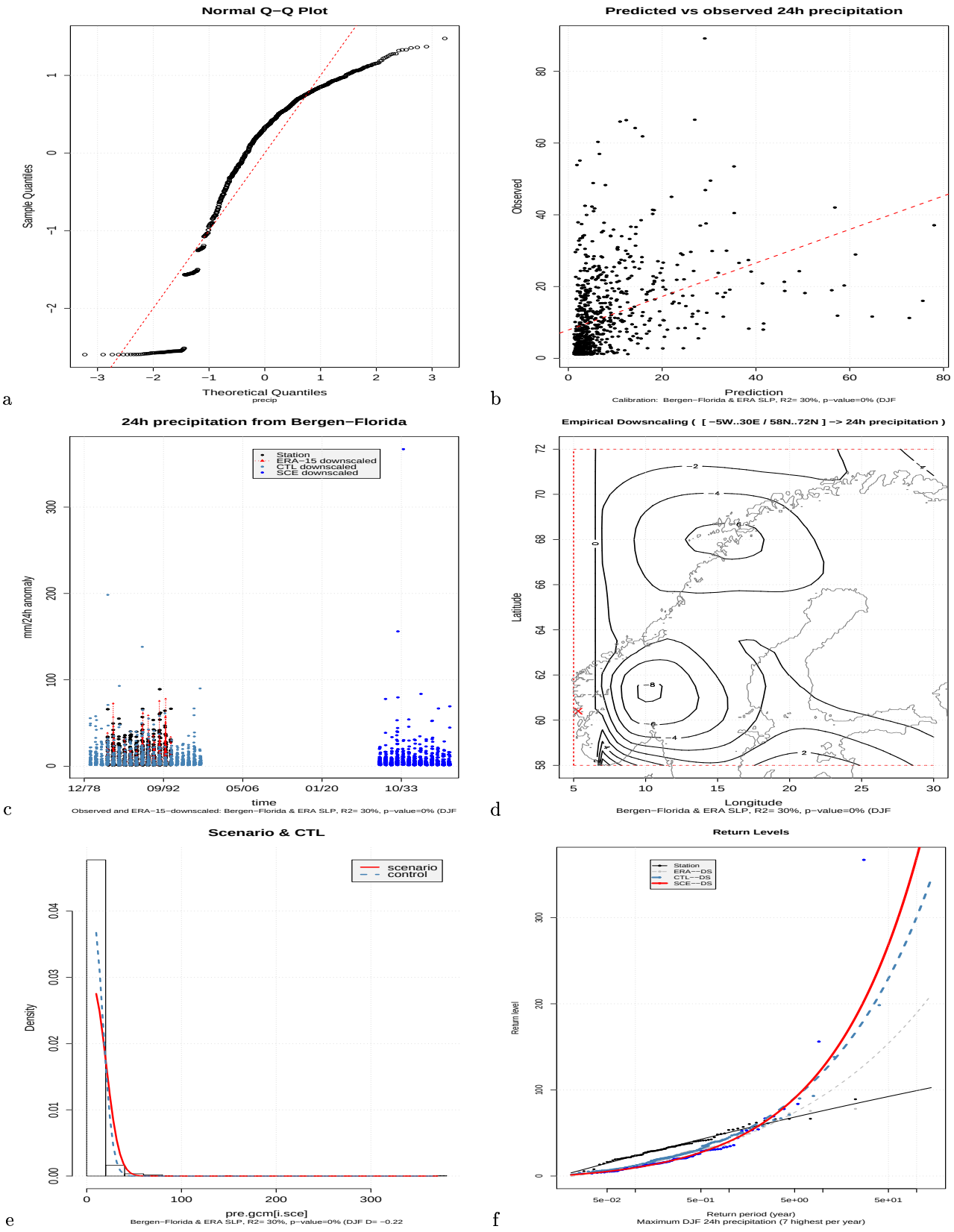

Figure 20. Downscaled results for daily mean winter precipitation at Bergen-Florida. (a) qq-plot of the precipitation series, (b) scatter plot between observations and (dependent) predictions, (c) the downscaled values, (d) geographical distribution of T(2m)-SLP field associated with precipitation variations in Bergen, (e) comparison between precipitation distributions in the control period and scenario, and (f) return-value analysis for daily mean winter precipitation in Bergen.

3.7 Mixed predictor fields

Figure 21 and 22 show the results for the downscaling of daily temperatures in Oslo and Bergen respectively. The scatter plots indicate a strong relationship between the local and regional variations and the ANOVA statistics (R^2 in the range of 85–88%, and a p-value ~ 0) suggest that the downscaling models capture most of the local winter temperature variations at these locations. The downscaled values (panel (c)) are also in good agreement with the observations, both for the dependent values, but also for the control period. These suggest that the downscaling models for daily values `clim.pact` are reliable is appropriate predictors are used. The large-scale anomalies associated with the temperature variations in Oslo and Bergen is also according to expectations: (i) the strongest temperature anomalies are situated near these locations and (ii) the SLP field suggests that these anomalies are coupled with an advection air from the west. In the case of Oslo, this circulation may be associated with the *Föhn* effect, whereas for Bergen the circulation pattern implies advection of mild maritime air from southwest.

Panel (e) shows the shift in the distribution of the winter temperature at Oslo and Bergen. The results for Oslo suggest a slight increase in variance and stronger shift in the upper tail. The asymmetric shift is clearer in Bergen (Figure 22e), where there is a more pronounced increase in the maximum values than in the minimum values. The stronger shift in the upper values can also be seen in the return-value analysis in panel (f): the return-values are similar in the control period and scenario for the same return-interval as long as the values are low. For extreme high temperatures, however, the analysis indicates a dramatic increase in frequency. It is apparent from the return-value analysis that the curves for the observations (black) and the downscaling of dependent variable (grey) are similar except for values corresponding to long return-intervals. At these long return-intervals, however, the estimates are associated with large uncertainties. Confidence limits are not shown in this plot. The return-value curve for the control period (steel blue) suggests that the model under-estimates the return values closer to the centre of the distribution. The analysis also over-estimates the return values for the Oslo temperature towards the higher tail (longer return intervals). The same results for the scenario suggest similar return values as observations nearer the centre of the distribution, but predicts much high return values for Oslo at longer return-intervals.

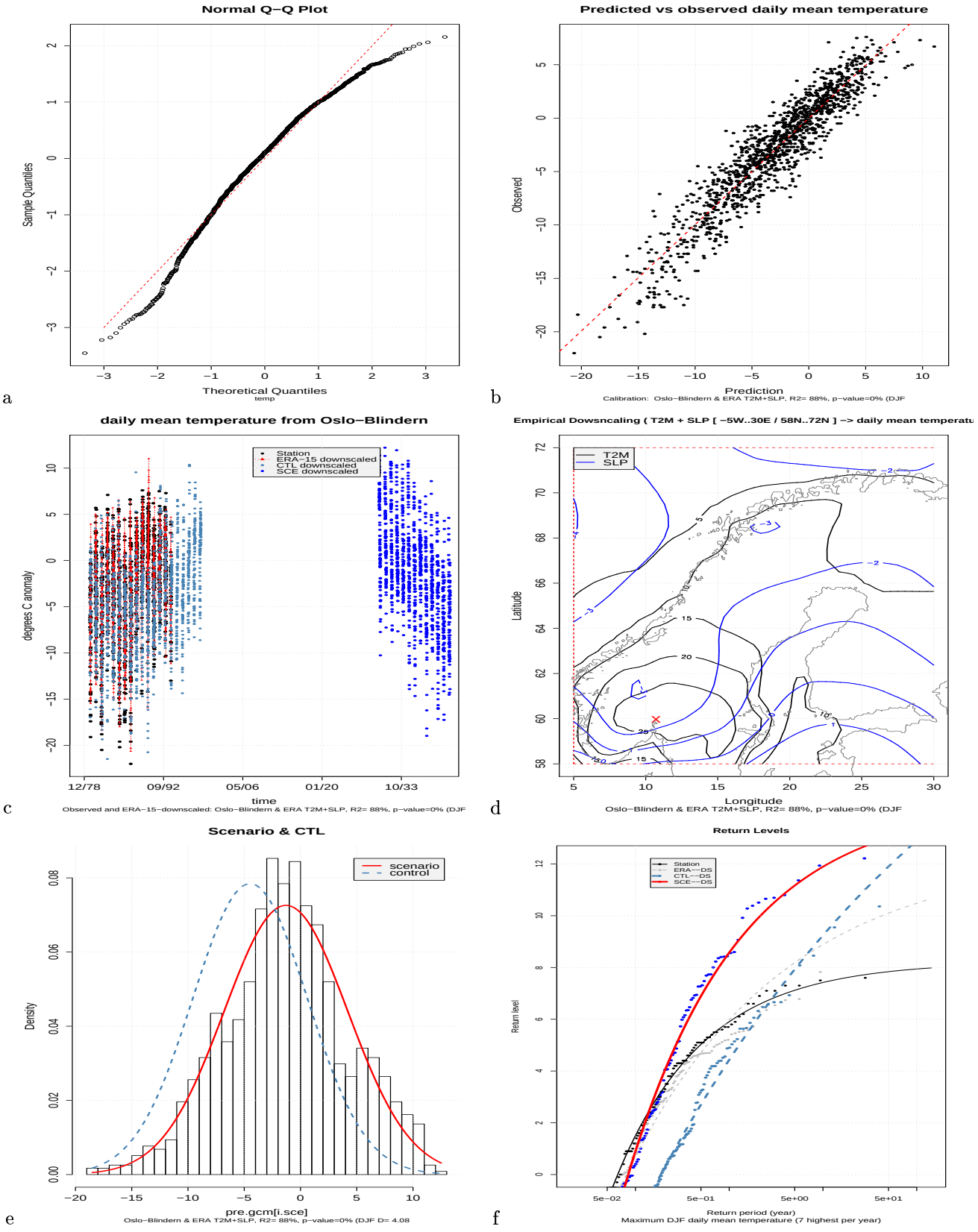

Figure 21. Downscaled results for daily mean winter temperature at Oslo-Blindern. (a) qq-plot of the temperature series, (b) scatter plot between observations and (dependent) predictions, (c) the downscaled values, (d) geographical distribution of T(2m)-SLP field associated with temperature variations in Oslo, (e) comparison between temperature distributions in the control period and scenario, and (f) return-value analysis for daily mean winter temperature in Oslo.

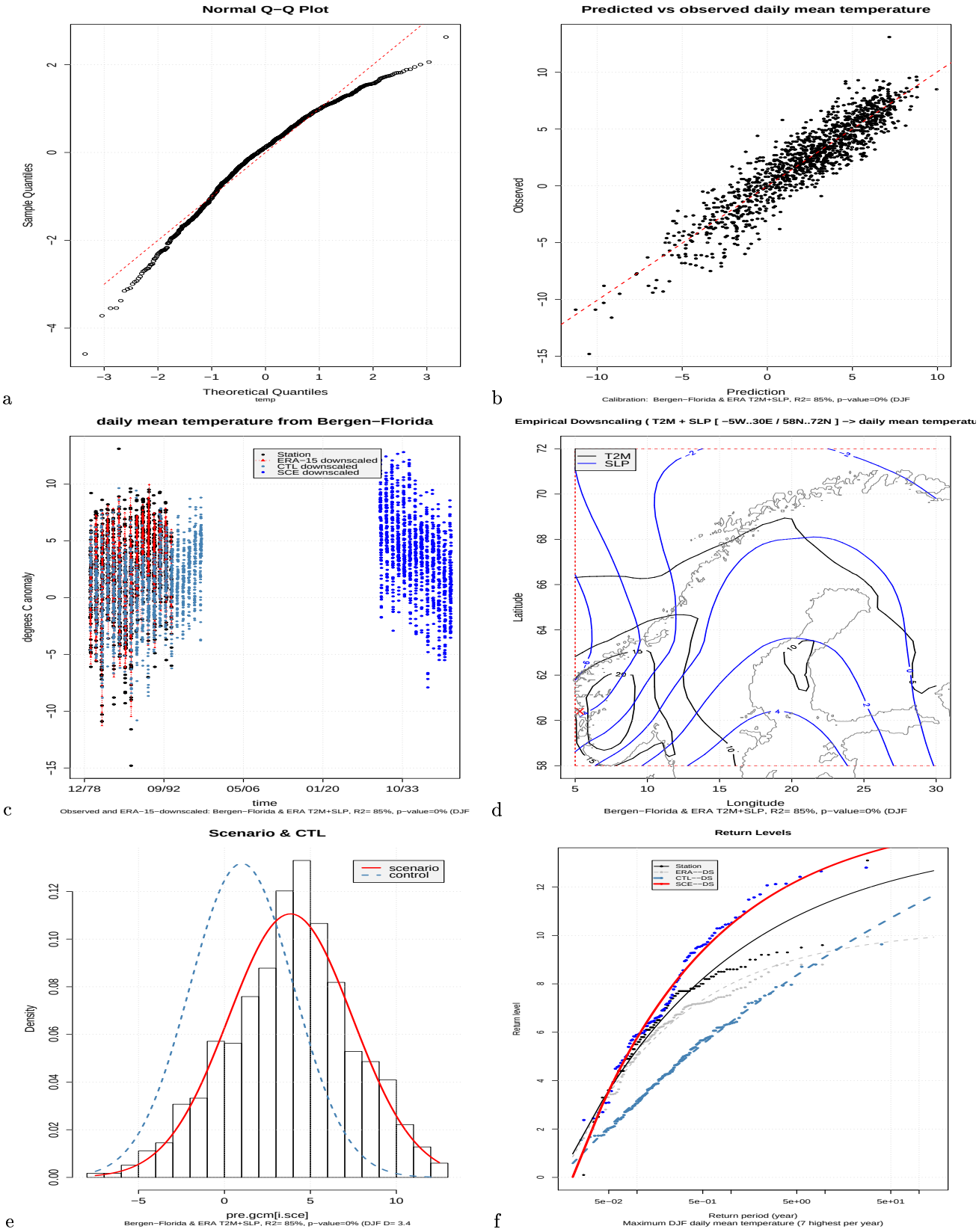

Figure 22. Downscaled results for daily mean winter temperature at Bergen-Florida. (a) qq-plot of the temperature series, (b) scatter plot between observations and (dependent) predictions, (c) the downscaled values, (d) geographical distribution of T(2m)-SLP field associated with temperature variations in Bergen, (e) comparison between temperature distributions in the control period and scenario, and (f) return-value analysis for daily mean winter temperature in Bergen.

3.8 Daily precipitation

The scatter plots in panels (b) further indicate that the relationship between the large-scale anomalies and the local precipitation is weak (ANOVA $R^2 = 0.40$, p-value ~ 0). The spatial patterns associated with the precipitation indicate an association between the winter temperature in Bergen and anomalous westerly geostrophic winds, whereas the winter temperature in Oslo is associated with more southeasterly circulation. The association between the local temperature variations and the large-scale circulation is therefore in accordance with the expectations.

A comparison between the histograms of the control period data and the scenario suggests a shift towards less future precipitation in Oslo, and a reduction in the variance in Bergen. The return value analysis also suggests a reduction in the frequency of extreme daily winter precipitation in Oslo, but the analysis indicates less change in Bergen. These scenarios are unexpected and contrary to the SLP-based results. It is again important to stress the fact that downscaling daily precipitation is problematic, partly due to fact that the local records are normally distributed and the timing discrepancy between predictand and predictor.

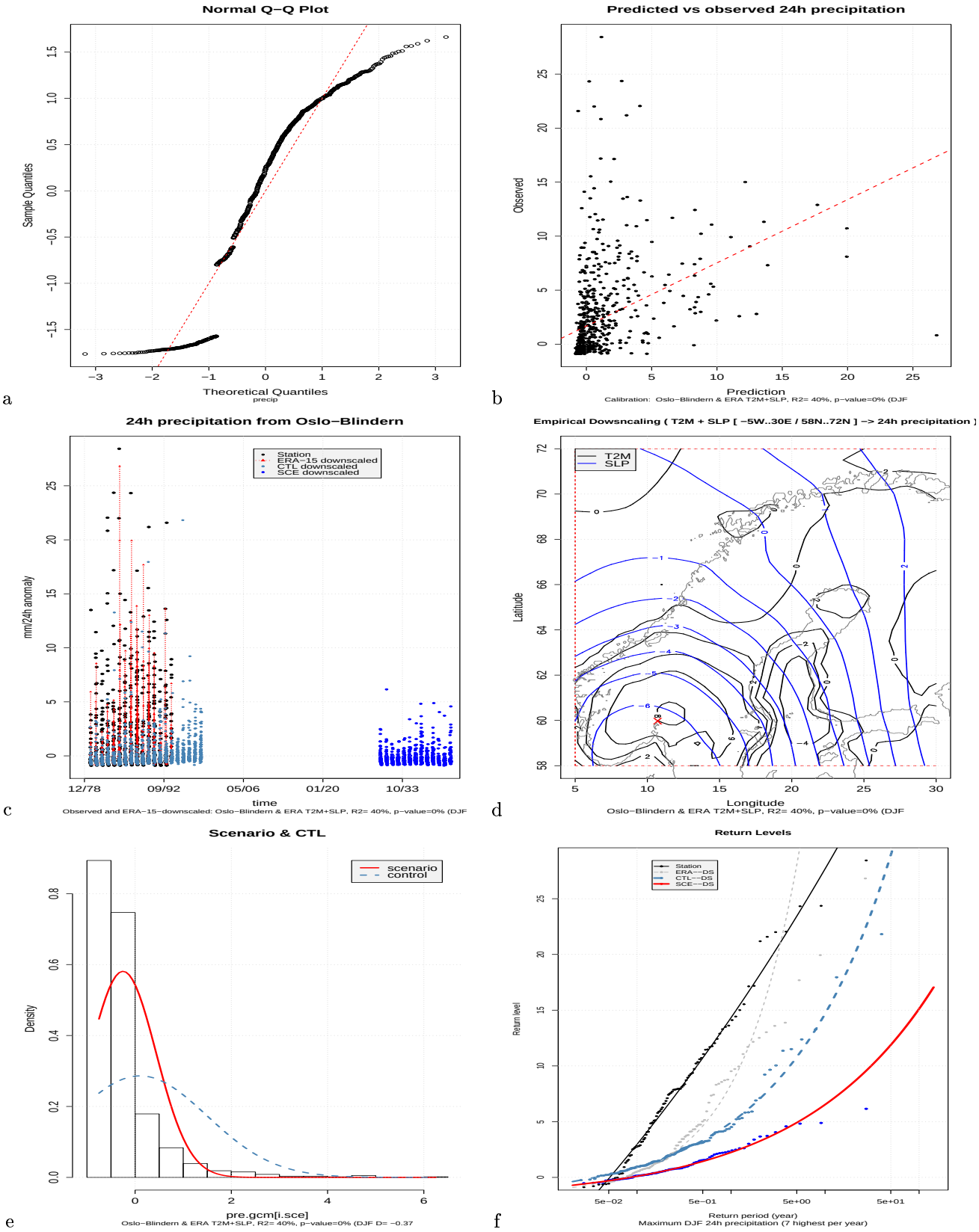

Figure 23. Downscaled results for daily mean winter precipitation at Oslo-Blindern. (a) qq-plot of the precipitation series, (b) scatter plot between observations and (dependent) predictions, (c) the downscaled values, (d) geographical distribution of T(2m)-SLP field associated with precipitation variations in Oslo, (e) comparison between precipitation distributions in the control period and scenario, and (f) return-value analysis for daily mean winter precipitation in Oslo.

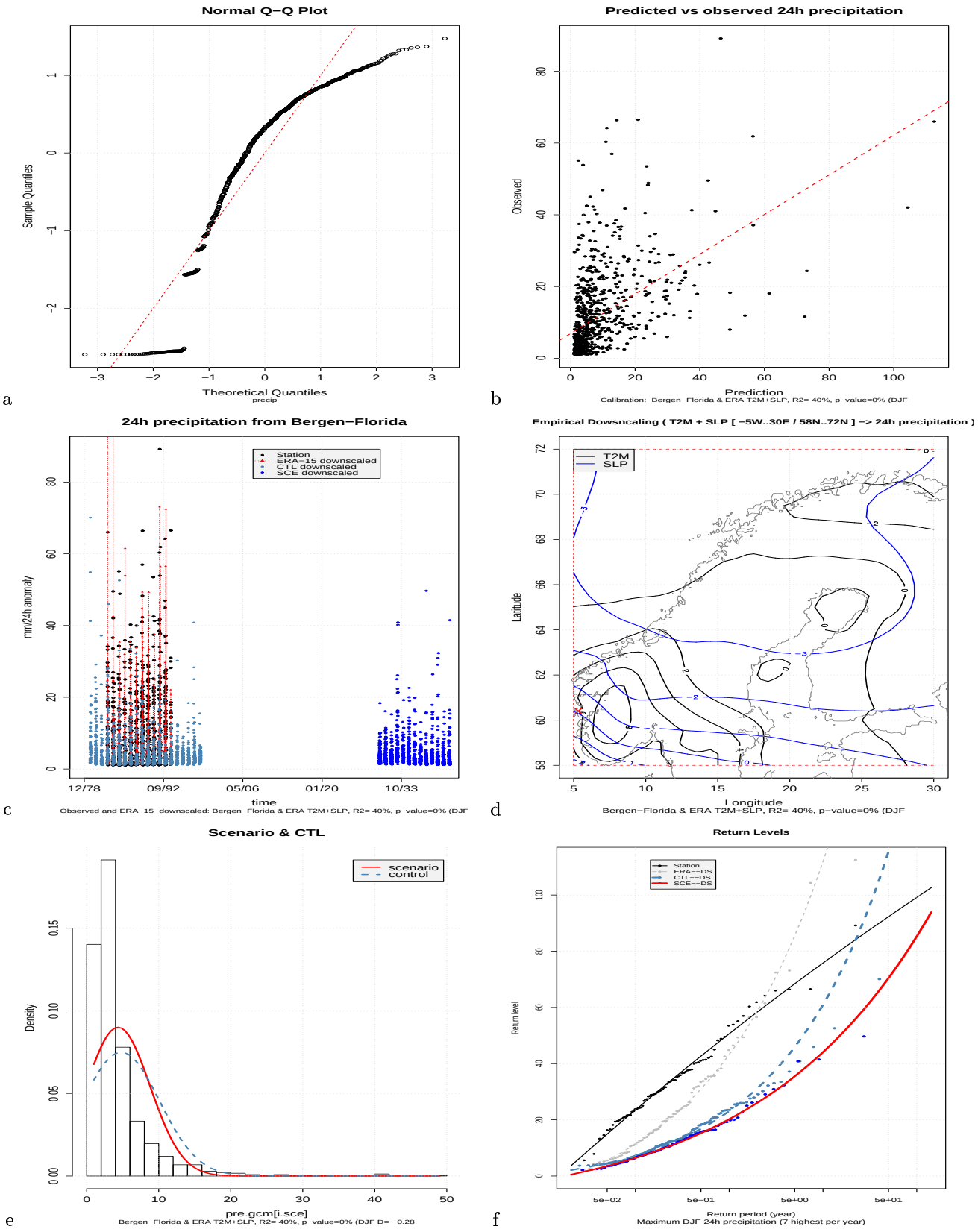

Figure 24. Downscaled results for daily mean winter precipitation at Bergen-Florida. (a) qq-plot of the precipitation series, (b) scatter plot between observations and (dependent) predictions, (c) the downscaled values, (d) geographical distribution of T(2m)-SLP field associated with precipitation variations in Bergen, (e) comparison between precipitation distributions in the control period and scenario, and (f) return-value analysis for daily mean winter precipitation in Bergen.

3.9 Using no transformation for precipitation

If the downscaling for daily precipitation is repeated with no transformation, then the R^2 value is slightly reduced, but there is still an indication that there is an association between the local winter precipitation and the large-scale circulation (Figure 25). Without the transformation, the analysis does not capture the high values and there are, according to the downscaled results, very few dry days (c). The analysis for the non-transformed data suggests a wetter future (e) and possibly a slight increase in the very heavy precipitation (f). However, there are severe problems associated with the downscaling of these results, and therefore these scenarios are not realistic.

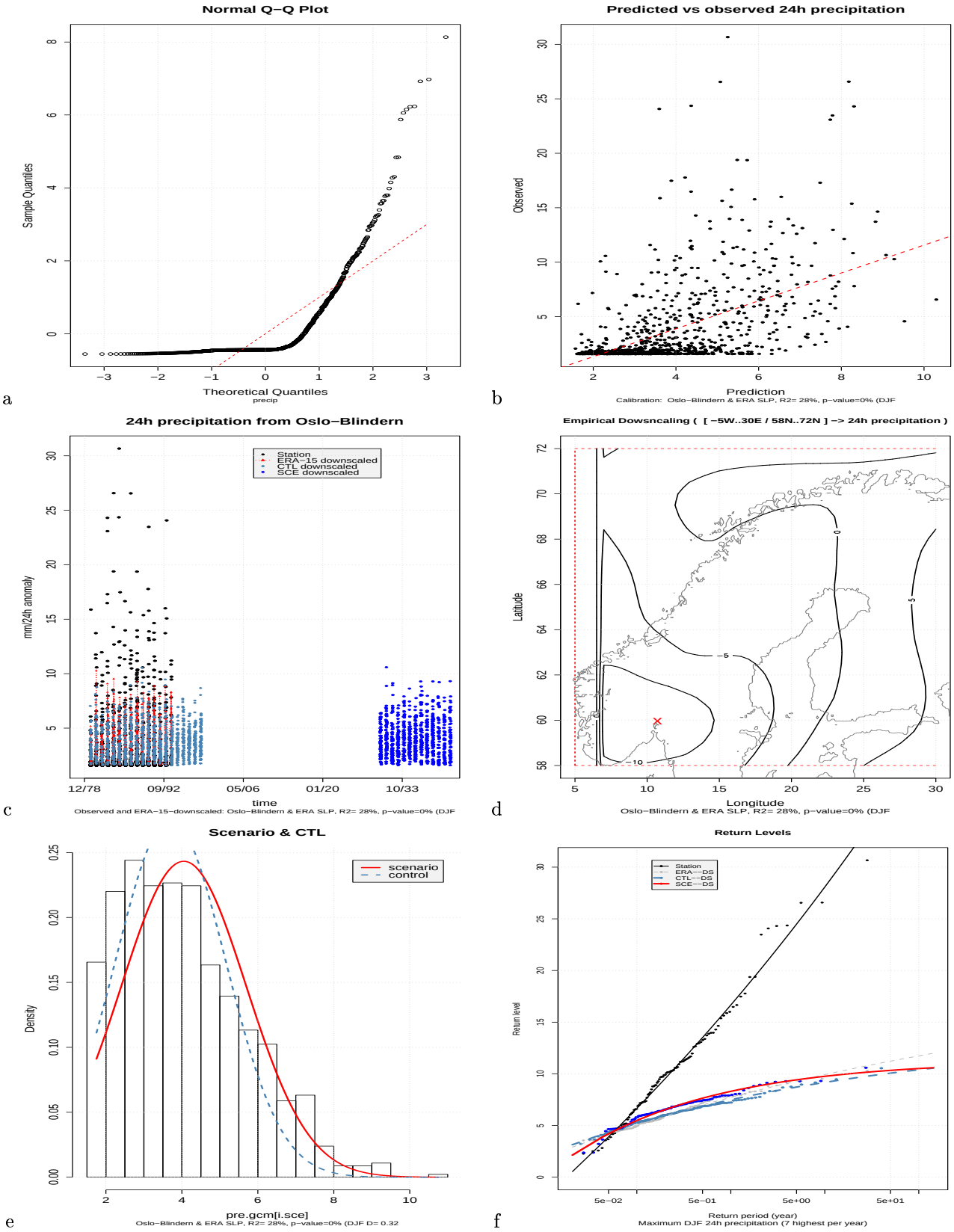

Figure 25. Downscaled results for daily mean winter precipitation at Oslo-Blindern using no transformation of the rainfall data. (a) qq-plot of the precipitation series, (b) scatter plot between observations and (dependent) predictions, (c) the downscaled values, (d) geographical distribution of T(2m)-SLP field associated with precipitation variations in Oslo, (e) comparison between precipitation distributions in the control period and scenario, and (f) return-value analysis for daily mean winter precipitation in Oslo.

3.10 Downscaling precipitation for wet days only

By removing the dry days and applying a log-transform, the rainfall is close to normally distributed. The threshold for "wet" day was in this case set to 6.0 mm (not shown). However, omitting the "dry" days weakens the statistical relationship between the local precipitation and the large-scale SLP anomalies: $R^2 = 0.04$, p-value=0.03. The maps of spatial anomalies suggested low pressure in the Arctic that was difficult to reconcile with a plausible physical mechanism. The observed and downscaled return value statistics were furthermore very different, implying that the downscaled results were unrealistic.

When a lower threshold was used (0.6 mm, Figure 26), the relationship between large and small scales was improved ($R^2 = 0.20$, p-value ~ 0) while the transformed data were fairly close to being normally distributed (a). The scatter plot (b), on the one hand, does not suggest that there is good correspondence between the ERA-15 downscaled and observed values and the downscaling underestimates the precipitation (c,f), but panel (d), on the other hand, suggests that the winter precipitation in Oslo is associated with local low pressure, which is in line with expectations. A comparison between the downscaled results for the control period and the future suggests a slight increase in the variance (e), and the return value statistics (f) suggest a slight increase in the frequency of heavy precipitation.

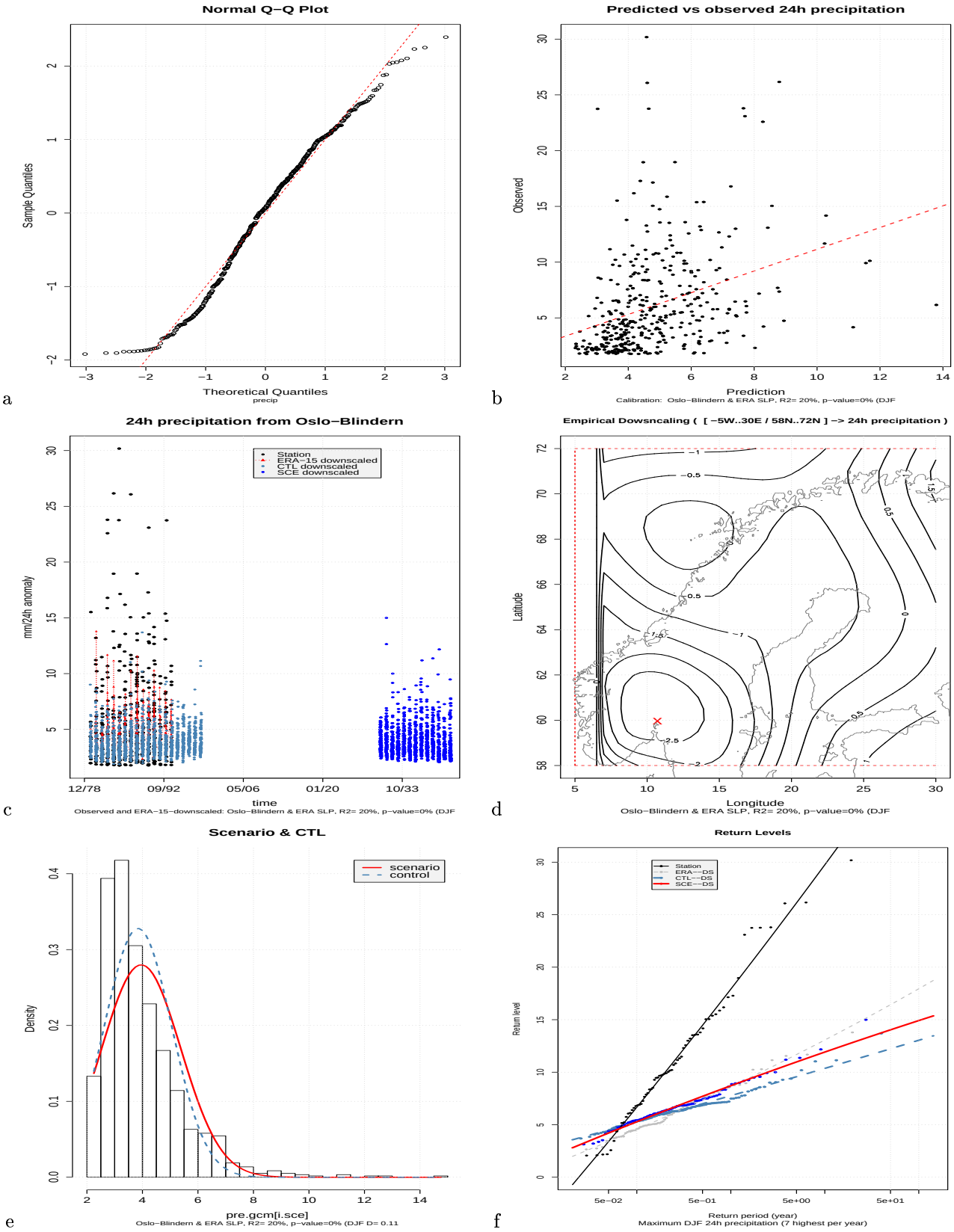

Figure 26. Downscaled results for daily mean winter precipitation at Oslo-Blindern using wet days only. (a) qq-plot of the precipitation series, (b) scatter plot between observations and (dependent) predictions, (c) the downscaled values, (d) geographical distribution of T(2m)-SLP field associated with precipitation variations in Oslo, (e) comparison between precipitation distributions in the control period and scenario, and (f) return-value analysis for daily mean winter precipitation in Oslo.

4 Discussion & Conclusions

The evaluation of `clim.pact` suggests that the analytical tool produces credible results for monthly and daily temperature. The tool is "generic" and can in principle be extended to any series that has a real association with the predictor field. The downscaling analysis was carried out for snow-depth, but the short length of the record and weak relationship between the January snow-depth and January large-scale anomalies limit the usefulness of the analysis. The downscaling of daily precipitation was hampered by severe problems due to the fact that the precipitation is non-Gaussian, a mismatch between the daily intervals for which the daily means of the predictor and the predictand are defined, and that relationships between large and small scales may not be linear. The analysis may be improved by incorporating analogue methods or neural nets (*Rummukainen*, 1997; *Zorita & von Storch*, 1997, 1999) (CHECK REFS!) into `clim.pact`. There are packages for `R` for neural nets (`nnet`).

Little reduction in variance associated with the use of common EOFs in agreement with observations made in *Benestad* (2001c).

Acknowledgments: This work was done under the Norwegian Regional Climate Development under Global Warming (RegClim) programme, and was supported by the Norwegian Research Council (Contract NRC-No. 120656/720) and the Norwegian Meteorological Institute. Dag Bjørge and Jan Erik Haugen provided the results from the dynamical downscaling with the HIRHAM model and Torill Engen Skaugen prepared the daily temperature and precipitation data. Colin Polsky tested and gave valuable feedback on the code used in `clim.pact`. The analysis was carried out using the `R` (*Ellner*, 2001; *Gentleman & Ihaka*, 2000) data processing and analysis language, which is freely available over the Internet (URL http://www.R-project.org/).

Appendix

5 Listing of R-code used to produce plots in this report.

6 R manual for clim.pact

References

Arrhenius, S.A., 1896. On the Influence of Carbonic Acid in the Air upon the Temperature of the Ground. *Philosophical Magazine and Journal of Science*, **41**, 237–276.

Barnett, T.P., 1999. Comparison of Near-Surface Air Temperature Variability in 11 Coupled Global Climate Models. *Journal of Climate*, **12**, 511–518.

Benestad, R.E., 1999. Solar Activity and Global Sea Surface Temperatures. *Astronomy & Geophysics*, **40**(June), 14 –17.

Benestad, R.E., 2000a. *Analysis of gridded sea level pressure and 2-meter temperature for 1873-1998 based on UEA and NCEP re-analysis II.* KLIMA 03/00. DNMI, PO Box 43 Blindern, 0313 Oslo, Norway.

Benestad, R.E., 2000b. *Future Climate Scenarios for Norway based on linear empirical downscaling and inferred directly from AOGCM results.* KLIMA 23/00. DNMI, PO Box 43 Blindern, 0313 Oslo, Norway.

Benestad, R.E., 2001a. The cause of warming over Norway in the ECHAM4/OPYC3 *GHG* integration. *International Journal of Climatology*, **21**, 371–387.

Benestad, R.E., 2001b. A comparison between two empirical downscaling strategies. *Int. J. Climatology*, **21**(November), 1645–1668. DOI 10.1002/joc.703.

Benestad, R.E., 2001c. Empirically downscaled multi-model ensemble temperature and precipitation scenarios for Norway. *Journal of Climate*, **15**(21), 3008–3027.

Benestad, R.E., 2002a. Empirically downscaled temperature scenarios for northern Europe based on a multi-model ensemble. *Climate Research*, **21 (2)**(June), 105–125.

Benestad, R.E., 2002b. What can present climate models tell us about climate change? *Climatic Change*, **accepted**.

Benestad, R.E., Hanssen-Bauer, I., & Førland, E.J., 2002. Empirically downscaled temperature scenarios for Svalbard. *Atmospheric Science Letters*, September 18, doi.10.1006/asle.2002.0051.

Bjørge, D., Haugen, J.E., & Nordeng, T.E., 2000. *Future Climate in Norway.* Research Report 103. DNMI, PO Box 43 Blindern, 0313 Oslo, Norway.

Christensen, O.B., J.H., Christensen, Machenhauer, B., & Botzet, M., 1998. Very High-Resolution Climate Simulations over Scandinavia - Present Climate. *Journal of Climate*, **11**, 3204–3229.

Coles, Stuart., 1999 (June). *Extreme value theory and applications.* Notes from a couse on EVT and applications presented at the 44th Reunião Annual da RBRAS e 8th SEAGRO, at Bucato, São Paulo, Brazil, 26-30 July, 1999. URL: http://www.maths.lancs.ac.uk/~coless.

Collins, M., 2000. Understanding Uncertainties in the response of ENSO to Greenhouse Warming. *Geophys. Res. Lett.*, **27**(21), 3509–3512.

Crane, R.G., & Hewitson, B.C., 1998. Doubled CO_2 Precipitation Changes for the Susquehanna Basin: Downscaling from the Genesis General Circulation Model. *International Journal of Climatology*, **18**, 65–76.

Ellner, Stephen P., 2001. Review of R, Version 1.1.1. *Bulletin of the Ecological Society of America*, **82**(2), 127–128.

Flury, B., 1988. *Common Principal Components and Related Multivariate Models.* Wiley Series in Probability and Mathematical Statistics. New York: Wiley.

Gentleman, R., & Ihaka, R., 2000. Lexical Scope and Statistical Computing. *Journal of Computational and Graphical Statistics*, **9**, 491–508.

Gibson, J. K., Kallberg, P., Uppala, S., Hernandez, A., Nomura, A., & Serrano, E., 1997. *ERA Description.* ERA Project Report Series. ECMWF.

Grotch, S., & MacCracken, M., 1991. The use of general circulation models to predict regional climate change. *Journal of Climate*, **4**, 286–303.

Heyen, H., Zorita, E., & von Storch, H., 1996. Statistical downscaling of monthly mean North Atlantic air-pressure to sea level anomalies in the Baltic Sea. *Tellus*, **48A**, 312–323.

IPCC., 2001. *IPCC WGI THIRD ASSESSMENT REPORT.* Summary for Policymakers. WMO.

Kalnay, E., Kanamitsu, M., Kistler, R., Collins, W., Deaven, D., Gandin, L., Iredell, M., Saha, S., White, G., Wollen, J., Zhu, Y., Chelliah, M., Ebisuzaki, W., Higgins, W., Janowiak, J., Mo, K.C., Ropelewski, C., Wang, J., Leetmaa, A., Reynolds, R., Jenne, R., & Joseph, D., 1996. The NCEP/NCAR 40-Year Reanalysis Project. *Bull. Amer. Meteor. Soc.*, **77**(3), 437–471.

Kaplan, A., Cane, M.A., Kushnir, Y., Clement, A.C., Blumenthal, M.B., & Rajagopalan, B., 1998.

Analyses of global sea surface temperature 1856-1991. *Journal of Geophysical Research*, **103**(C9), 18,567–18,589.

Kidson, J.W., & Thompson, C.S., 1998. A Comparison of Statistical and Model-Based Downscaling Techniques for Estimating Local Climate Variations. *Journal of Climate*, **11**, 735–753.

Lorenz, E., 1967. *The Nature and Theory of the General Circulation of the Atmosphere.* Publication 218. WMO.

Meehl, G.A., Collins, W.D., Boville, B.A., Kiehl, J.T., Wigley, T.M.L., & Arblaster, J.M., 2000. Response of the NCAR Climate System Model to Increased CO_2 and the Role of Physical Processes. *Journal of Climate*, **13**(June), 1879–1898.

North, G.R., Bell, T.L., & Cahalan, R.F., 1982. Sampling Errors in the Estimation of Empirical Orthogonal Functions. *Monthly Weather Review*, **110**, 699–706.

Parkinson, C.L., Rind, D., Healy, R.J., & Martinson, D.G., 2001. The impact of Sea Ice Concentration Accuracy on Climate Model Simulations with the GIS GCM. *Journal of Climate*, **14**(June), 2606–2623.

Press, W.H., Flannery, B.P., Teukolsky, S.A., & Vetterling, W.T., 1989. *Numerical Recipes in Pascal.* Cambridge University Press.

Rummukainen, M., 1997. *Methods for Statistical downscaling of GCM simulations.* SWECLIM 80. SMHI.

Sengupta, S., & Boyle, J. S., 1998. Using Common Principal Components in Comparing GCM Simulations. *Journal of Climate*, **11**, 816–830.

Sengupta, S. K., & Boyle, J. S., 1993 (November). *Statistical Intercomparison of Global Climate Models: A Common Principal Component Approach.* Tech. rept. 13. PCMDI, Lawrence Livermore National Laboratory, California, USA, [http://www-pcmdi.llnl.gov/pcmdi/pubs/pdf/13.pdf].

Shindell, D.T., Schmidt, G.A., Miller, R.L., & Rind, D., 2001. Northern Hemipshere winter climate response to greenhouse gas, ozone, solar, and volcanic forcing. *Journal of Geophysical Research*, **106**(D7), 7193–7210.

Tuomenvirta, H., Drebs, A., Førland, E., Alexandersson, O.E. Tveitoand H., Laursen, E.V., & Jónsson, T., 2001. *Nordklim data set 1.0.* KLIMA 08/01. met.no, P.O.Box 43 Blindern, N-0313 Oslo, Norway.

Wilby, R.L., Hassan, H., & Hanaki, Keisuke., 1998. Statistical downscaling of hydrometeorological variables using general circulation model output. *Journal of Hydrology*, **205**, 1–19.

Wilks, D.S., 1995. *Statistical Methods in the Atmospheric Sciences.* Orlando, Florida, USA: Academic Press.

Zorita, E., & von Storch, H., 1997. *A survey of statistical downscaling results.* Tech. rept. 97/E/20. GKSS.

Zorita, E., & von Storch, H., 1999. The Analog Method as a Simple Statistical Downscaling Technique: Comparison with More Complicated Methods. *Journal of Climate*, **12**, 2474–2489.